which was reduced by treatment with TACI siRNA and heparitinase, though APRIL also increased the IgG/IgM ratio, which was reduced by treatment with heparitinase but not by TACI siRNA (Figure 2B, lane 6). In agreement with the data that APRIL-induced IgA CSR and production was abolished by TACI siRNA, flow cytometric analysis showed that 9.8% of untreated B cells were positive for IgA after 48-hour stimulation with APRIL to a level comparable to that of BAFF stimulation (Figure 2C). In contrast, only 2.3% or 2.8% of B cells were positive for IgA after treatment with heparitinase or TACI siRNA, respectively (Figure 2C). It should be noted that agonistic anti-TACI mAb itself failed to elicit B-cell responses (Figure 2A, lane 7). Thus, these results suggest that HSPG is essential for APRIL-induced B-cell responses and that TACI positively regulates APRIL-induced IgA CSR and production but not B-cell proliferation or IgG production. APRIL binding to TACI and HSPG is indispensable for IgA production.

TACI-dependent PKA activation is induced by APRIL but not by BAFF

Nuclear factor-κ B (NF-κB) signaling has 2 pathways, canonical NF-κB1 and noncanonical NF-κB2 pathway, as evidenced by the nuclear translocation of p50/RelA (p65) and p52/RelB complexes,[23,24] respectively. Stimulation with CD40L and BAFF preferentially activates the noncanonical pathway responsible for B-cell responses, such as cell proliferation, immunoglobulin production, and AID-mediated CSR.[25] As shown in Figure 3, NF-κB1 translocation induced by BAFF, APRIL, and agonistic anti-TACI mAb (lanes 3-5) was greatly diminished by TACI siRNA (lanes 15-17) and by heparitinase treatment (lanes 21-23). Although NF-κB2 translocation was induced by BAFF and APRIL (lanes 3-4), the translocation by BAFF but not by APRIL was greatly enhanced by TACI siRNA (lane 15), which was irrelevant to the state of HSPG (lane 21). On the other hand, denaturation of HSPG diminished APRIL-induced NF-κB2 translocation (lane 4 vs lane 10), which was not influenced by TACI siRNA (lane 22 vs lane 16). Moreover, the induction of AID paralleled the behavior of NF-κB2 translocation, indicating that APRIL-induced NF-κB1 translocation is dependent on TACI and that APRIL/HSPG binding is necessary for NF-κB2 translocation and AID induction.

Next, we examined the status of PKA activation because PKA plays a critical role in the posttranslational regulation of AID activity and in the induction of immunoglobulin CSR through the phosphorylation of AID.[26,27] PKA phosphorylation was clearly observed in response to CD40L, BAFF, and APRIL (lanes 2-4). When treated with heparitinase, PKA phosphorylation was blocked in response to APRIL but not to CD40L or BAFF (lanes 8-10). Loss of PKA phosphorylation in TACI knockdown B cells was observed in APRIL stimulation but not in BAFF (lanes 15-16). Thus, impaired APRIL-induced IgA secretion (Figure 2A) in TACI knockdown B cells correlated with impaired PKA phosphorylation but not AID induction or NF-κB2 translocation. These results suggest that APRIL-induced PKA activation requires TACI and HSPG ligation and that TACI may play a pivotal role in APRIL-induced IgA production by regulating AID activity through PKA phosphorylation.

Simultaneous coligation of TACI and HSPG is required for PKA activation and subsequent IgA production

To confirm the mutual cooperation between TACI and HSPG in APRIL-induced IgA production, we tried to mimic the coligation of TACI and HSPG with specific antibodies and their second antibody instead of APRIL ligation. Figure 4 shows that phosphorylation of PKA (Figure 4A) and IgA secretion (Figure 4B) were induced when TACI and HSPG were coligated simultaneously, indicating that APRIL binding to TACI and HSPG is essential for IgA production. We then examined whether the defective PKA activation was sufficient to explain the lack of APRIL-induced IgA secretion in TACI knockdown B cells by testing whether constitutive PKA activity could compensate for the defect of TACI signaling. For constitutive activation of PKA, we used 8-bromo-cAMP, a cell-permeable cAMP analog known to act as a potent inducer of PKA activation.[28] As expected, cAMP administration resulted in PKA phosphorylation even in the absence of TACI (Figure 5A), which in turn recovered APRIL-induced IgA secretion (Figure 5B), indicating the essential role of TACI-mediated PKA activation in APRIL-induced IgA production. Thus, HSPG-mediated AID induction was insufficient for IgA production and TACI-mediated PKA activation was indispensable for APRIL-induced IgA production. These results suggest that the defective secretion of IgA by TACI knockdown B cells was caused by insufficient PKA activation and that TACI and HSPG synergistically mediated a signal for PKA activation and IgA production.

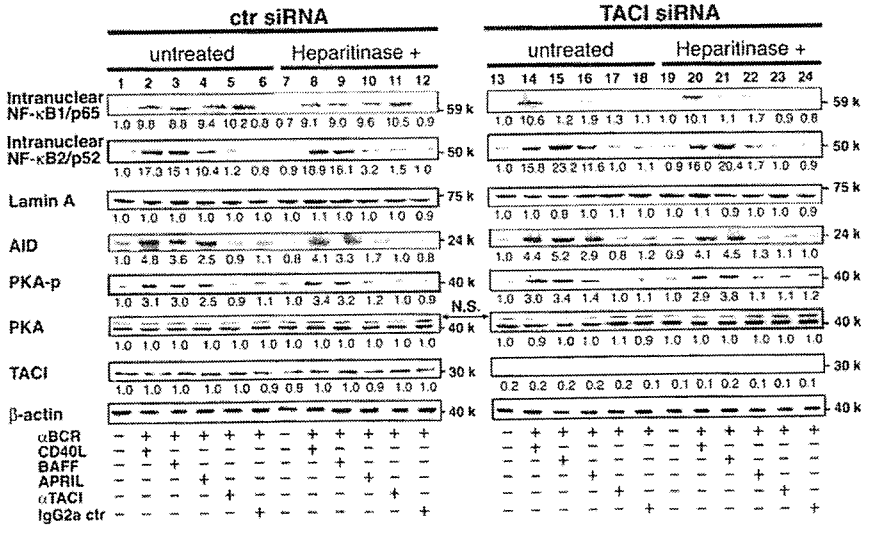

Figure 3. Effects of TACI siRNA and heparitinase on APRIL- and BAFF-induced NF-κB2 and AID expression and PKA phosphorylation. B cells pretreated with control siRNA, TACI siRNA, or heparitinase (10 U/mL) were cultured with anti-BCR antibodies (anti-Igκ and anti-Igλ, 0.5 μg/mL each), CD40L (2 μg/mL), BAFF (4 μg/mL), APRIL (8 μg/mL), anti-TACI mAb (11H3; 5 μg/mL), or control mouse IgG2a (5 μg/mL) in the presence of TGF-β (1 ng/mL). Incubation times differed with individual probes: 30 minutes for NF-κB1/p65 and TACI, 6 hours for NF-κB2/p52, 72 hours for AID, and 45 minutes for PKA phosphorylation. Nuclear extracts and cell lysates were prepared and subjected to immunoblot analysis. Density of each band was analyzed (LumiVision analyzer) and was presented as relative fold of the minimum density in each panel. Data are representative of 3 independent experiments with similar results.

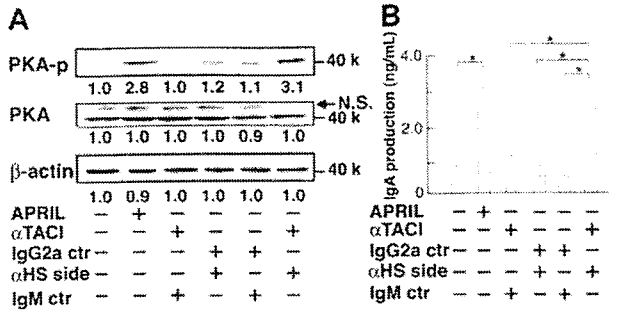

Figure 4. Effects of coligation of TACI and HSPG on PKA phosphorylation and IgA production. (A) IgA-negative B cells were cultured with anti-TACI mAb (11H3), anti–heparan sulfate side chain mAb (10E4), mouse IgG2a, or mouse IgM (5 μg/mL each) for 45 minutes. Then anti–mouse Igκ (1 μg/mL) antibody was added to establish the cross-linking of cell-bound mAbs. APRIL (8 μg/mL) was used as a positive control. After 45-minute incubation, cell lysates were prepared and subjected to immunoblot analysis (B) IgA concentrations in culture supernatant were measured by ELISA after 10 days. Data are mean ± SD. $^*P < .05$ Data are representative of 3 independent experiments with similar results.

Discussion

In the present study, we showed that TACI was a positive regulator for APRIL-induced IgA production and a negative regulator for BAFF-induced B-cell responses such as B-cell proliferation and production of IgA and IgG in human peripheral blood B cells in vitro. In addition, we demonstrated that HSPG was essential for APRIL-induced B-cell responses, including the activation of noncanonical NF-κB2 pathway and the induction of AID, whereas TACI contributed less to APRIL-induced B-cell responses except for PKA activation and IgA production.

The positive role of TACI and APRIL in IgA production appears to be important in vivo because TACI and APRIL knockout mice showed reduced levels of serum IgA and deficient IgA responses to mucosally immunized antigens, and old APRIL transgenic mice showed increased levels of serum IgA.[13,14,19,29,30] In addition, defects in TACI have been reported in patients with IgA deficiency and CVID.[16,17] Why is APRIL/TACI rather than BAFF/BAFF-R dominant in IgA production in vivo? The reason might be explained by the localization of IgA-producing cells and TACI-expressing cells. Most IgA antibody is synthesized by mucosal plasma cells associated with lymphoid tissue, gut-associated B cells, and B-1 B cells.[31,32] It has been reported that TACI but not BAFF-R is highly expressed in human small intestine[3,7] and that murine B-1 B cells bind strongly and specifically to APRIL.[30]

We observed that TACI stimulation itself could not induce B-cell activation (Figure 2A); thus, it is unlikely that TACI alone is involved directly in APRIL-induced IgA production. In addition, a previous report described a deficiency of immunoglobulin CSR in TACI knockout B cells after stimulation with APRIL in mice,[29] which is almost similar to the result described here for IgA production with TACI knockdown, in addition to the up-regulation of AID and the mild reduction in IgG. These observations suggest that HSPG plays a major role in APRIL-induced immunoglobulin CSR and that the synergistic ability of TACI is responsible for IgA CSR with HSPG. In this regard, we demonstrated that the coligation of TACI and HSPG by specific mAbs clearly induced IgA production instead of APRIL (Figure 4). However, because HSPG is widely expressed throughout the B-cell lineage as transmembrane proteins such as CD44 and syndecan 1[8,33] and the expression of TACI varies after activation,[34] TACI seems to play a critical role in APRIL-induced IgA production under physiological conditions.

We showed here that although AID was expressed at comparable levels in B cells with TACI and control siRNA (Figure 3), APRIL-induced IgA secretion was impaired by TACI siRNA whereas IgG secretion was slightly reduced compared with siRNA control (Figure 2). It is possible that the dissimilarity in TACI-mediated immunoglobulin responses resulted from differences in the threshold of PKA-mediated phosphorylation that affect AID functionality to induce immunoglobulin CSR. Castigli et al[29] demonstrated the preferential induction of molecular events in IgG CSR rather than IgA CSR in TACI knockout B cells in response to APRIL. Basu et al[26] identified several phosphorylation sites on AID responsible for IgG CSR and demonstrated marked abrogation of IL-4–, TGF-β–, and CD40-induced IgA CSR by PKA inhibition, suggesting that IgA CSR might require more potent PKA activity than IgG CSR. Our finding that activated PKA by a cAMP analog has a capacity sufficient to induce APRIL-induced IgA secretion, despite the absence of TACI (Figure 5), suggests that AID is induced by the binding of APRIL to HSPG and becomes activated after TACI-dependent proper regulation of PKA.

It has been reported that mouse splenic B cells proliferate in response to a form of APRIL that cannot bind HSPG or APRIL in the presence of heparin.[9] However, we could not observe APRIL-induced proliferation of human peripheral blood B cells treated with heparitinase (Figure 2A) and cultured in the presence of heparin (data not shown). Perhaps these results were different because the APRIL splice variant present in mice can bind to mouse BAFF-R though it does not exist in humans and because human APRIL does not interact with human BAFF-R, as reported recently.[35] In addition, it has been reported that TACI knockout B cells do not show IgA CSR and production in response to BAFF in mice.[29] Given that we could not observe an obvious defect in IgA secretion by TACI knockdown B cells in response to BAFF, the different results might be attributed, at least in part, to differences between murine splenic B cells and human peripheral blood B cells.

Although normal humoral responses to TD-Ags and B-cell maturation have been observed in TACI knockout mice, humoral responses to TI-Ags were impaired.[13] B cells responding to TI-Ags reside largely in marginal zone (MZ) B-cell and B-1 B-cell compartments.[36,37] It has been reported that TACI is highly expressed on mouse MZ B cells[34] and that B-1 B cells bind strongly and specifically to APRIL.[30] Thus, it is possible that adequate APRIL binding to TACI and HSPG on these B cells is a more likely explanation of the effects observed in TACI knockout mice. MZ B

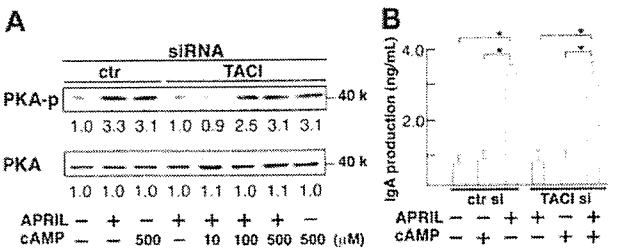

Figure 5. Recovery of APRIL-induced IgA production by activation of PKA in the absence of TACI. Controller TACI siRNA-transfected B cells were cultured with different doses of cAMP analog 8-bromo-cAMP (A; 10, 100 or 500 μM) (B; 500 μM) for 2 hours. Cells were further cultured in the presence of APRIL (8 μg/mL), anti-BCR antibodies (anti-Igκ and anti-Igλ, 0.5 μg/mL each), and TGF-β (1 ng/mL). PKA phosphorylation by immunoblotting (A) or IgA secretion by ELISA (B) was evaluated after 45 minutes or 10 days culture, respectively. Data are mean ± SD. $^*P < .05$. Data are representative of 3 independent experiments with similar results.

cells and B-1 B cells can readily undergo CSR from IgM to IgG or IgA in a T cell–independent fashion.[38] Recent studies suggest that T cell–independent CSR requires the interaction of B cells with dendritic cells.[21,39] APRIL secreted from dendritic cells by TI-Ags might enable proper antibody production from MZ and B-1 B cells.

Homozygous and heterozygous mutations in TNFRSF13B are associated with the loss of TACI function, as reported in patients with CVID and IgA deficiency.[16,17] Conversely, strong induction of mature B-cell proliferation, B-cell hyperresponsiveness, lymphadenopathy, and systemic lupus erythematosus nephritis was observed in TACI knockout mice.[13-15] However, only a minority of CVID patients showed signs of autoimmunity or lymphoproliferation.[16] In theory, it could still be possible that HSPG or TACI is expressed on human B cells at levels different from those on murine B cells, reflecting differences in severity. As discussed, TACI is a negative regulator for BAFF-induced B-cell responses and a positive regulator of APRIL-induced IgA production and humoral responses to TI-Ags in collaboration with HSPG. Thus, immunoglobulin deficiency other than IgA observed in CVID patients with TACI defects might have resulted from other CVID disease-specific factors.

In conclusion, the present study identified bilateral regulatory roles of TACI B-cell responses and their importance, especially in IgA production in collaboration with HSPG. These new findings should enhance our understanding of mucosal immune system and humoral responses to TI-Ags.

Acknowledgments

This work was supported by Dokkyo University School of Medicine Investigator-Initiated Research grant 2005-01-8 (D.S.); a grant for Hi-Tech Research from Dokkyo Medical University School of Medicine (T.K.); Grant-in-Aid for Scientific Research (C) KAKENHI 16590410 (T.K.) from the Ministry of Education, Culture, Sports, Science and Technology of Japan; Health and Labour Sciences Research Grants for Research on Health Sciences focusing on Drug Innovation from the Ministry of Health, Labour, and Welfare of Japan (T.K.); and the Science Research Promotion Fund from the Promotion and Mutual Aid Corporation for Private Schools of Japan (T.K.).

We thank Dr H. Karasuyama for the pBCMGSneo expression vector, Dr S. F. Schlossman for helpful discussion, and Y. Nitta for secretarial assistance. We also thank the Laboratory Animal Research Center and Laboratory of Analytical Instruments, Institute for Medical Science, Dokkyo Medical University, for the use of their facilities and the Japanese Red Cross Tochigi Blood Center for leukopaks. We thank Dr F. G. Issa for the critical reading of the manuscript.

Authorship

Contribution: D.S. performed the experiments and wrote the paper; H.H. analyzed the data and participated in the writing of the paper; Y.K. collected the data; H.K. analyzed the data; K.O. contributed vital new reagents; and T.K. designed the research protocol and wrote the paper.

Conflict-of-interest disclosure: The authors declare no competing financial interests.

Correspondence: Tetsuji Kobata, Department of Immunology, Dokkyo Medical University School of Medicine, 880 Kitakobayashi, Mibu, Tochigi 321-0293, Japan; tkobata@dokkyomed.ac.jp.

References

1. Mackay F, Schneider P, Rennert P, Browning J. BAFF AND APRIL: a tutorial on B cell survival. Annu Rev Immunol. 2003;21:231-264.
2. Dillon SR, Gross JA, Ansell SM, Novak AJ. An APRIL to remember: novel TNF ligands as therapeutic targets. Nat Rev Drug Discov. 2006;5:235-246.
3. von Bulow GU, Bram RJ. NF-AT activation induced by a CAML-interacting member of the tumor necrosis factor receptor superfamily. Science. 1997;278:138-141.
4. Marsters SA, Yan M, Pitti RM, Haas PE, Dixit VM, Ashkenazi A. Interaction of the TNF homologues BLyS and APRIL with the TNF receptor homologues BCMA and TACI. Curr Biol. 2000;10:785-788.
5. Yu G, Boone T, Delaney J, et al. APRIL and TALL-I and receptors BCMA and TACI: system for regulating humoral immunity. Nat Immunol. 2000; 1:252-256.
6. Yan M, Brady JR, Chan B, et al. Identification of a novel receptor for B lymphocyte stimulator that is mutated in a mouse strain with severe B cell deficiency. Curr Biol. 2001;11:1547-1552.
7. Thompson JS, Bixler SA, Qian F, et al. BAFF-R, a newly identified TNF receptor that specifically interacts with BAFF. Science. 2001;293:2108-2111.
8. Hendriks J, Planelles L, de Jong-Odding J, et al. Heparan sulfate proteoglycan binding promotes APRIL-induced tumor cell proliferation. Cell Death Differ. 2005;12:637-648.
9. Ingold K, Zumsteg A, Tardivel A, et al. Identification of proteoglycans as the APRIL-specific binding partners. J Exp Med. 2005;201:1375-1383.
10. Schiemann B, Gommerman JL, Vora K, et al. An essential role for BAFF in the normal development of B cells through a BCMA-independent pathway. Science. 2001;293:2111-2114.
11. Sasaki Y, Casola S, Kutok JL, Rajewsky K, Schmidt-Supprian M. TNF family member B cell-activating factor (BAFF) receptor-dependent and -independent roles for BAFF in B cell physiology. J Immunol. 2004;173:2245-2252.
12. Shulga-Morskaya S, Dobles M, Walsh ME, et al. B cell-activating factor belonging to the TNF family acts through separate receptors to support B cell survival and T cell-independent antibody formation. J Immunol. 2004;173:2331-2341.
13. von Bulow GU, van Deursen JM, Bram RJ. Regulation of the T-independent humoral response by TACI. Immunity. 2001;14:573-582.
14. Yan M, Wang H, Chan B, et al. Activation and accumulation of B cells in TACI-deficient mice. Nat Immunol. 2001;2:638-643.
15. Seshasayee D, Valdez P, Yan M, Dixit VM, Tumas D, Grewal IS. Loss of TACI causes fatal lymphoproliferation and autoimmunity, establishing TACI as an inhibitory BLyS receptor. Immunity. 2003; 18:279-288.
16. Salzer U, Chapel HM, Webster AD, et al. Mutations in TNFRSF13B encoding TACI are associated with common variable immunodeficiency in humans. Nat Genet. 2005;37:820-828.
17. Castigli E, Wilson SA, Garibyan L, et al. TACI is mutant in common variable immunodeficiency and IgA deficiency. Nat Genet. 2005;37:829-834.
18. Stein JV, Lopez-Fraga M, Elustondo FA, et al. APRIL modulates B and T cell immunity. J Clin Invest. 2002;109:1587-1598.
19. Castigli E, Scott S, Dedeoglu F, et al. Impaired IgA class switching in APRIL-deficient mice. Proc Natl Acad Sci U S A. 2004;101:3903-3908.
20. Avery DT, Kalled SL, Ellyard JI, et al. BAFF selectively enhances the survival of plasmablasts generated from human memory B cells. J Clin Invest. 2003;112:286-297.
21. Litinskiy MB, Nardelli B, Hilbert DM, et al. DCs induce CD40-independent immunoglobulin class switching through BLyS and APRIL. Nat Immunol. 2002;3:822-829.
22. Hase H, Kanno Y, Kojima M, et al. BAFF/BLyS can potentiate B-cell selection with the B-cell coreceptor complex. Blood. 2004;103:2257-2265.
23. Beinke S, Ley SC. Functions of NF-κB1 and NF-κB2 in immune cell biology. Biochem J. 2004;382: 393-409.
24. Bonizzi G, Karin M. The two NF-κB activation pathways and their role in innate and adaptive immunity. Trends Immunol. 2004;25:280-288.
25. Zarnegar B, He JQ, Oganesyan G, Hoffmann A, Baltimore D, Cheng G. Unique CD40-mediated biological program in B cell activation requires both type 1 and type 2 NF-κB activation pathways. Proc Natl Acad Sci U S A. 2004;101:8108-8113.
26. Basu U, Chaudhuri J, Alpert C, et al. The AID antibody diversification enzyme is regulated by protein kinase A phosphorylation. Nature. 2005;438: 508-511.
27. Pasqualucci L, Kitaura Y, Gu H, Dalla-Favera R. PKA-mediated phosphorylation regulates the function of activation-induced deaminase (AID) in B cells. Proc Natl Acad Sci U S A. 2006;103:395-400.
28. Hei YJ, MacDonell KL, McNeill JH, Diamond J. Lack of correlation between activation of cyclic AMP-dependent protein kinase and inhibition of contraction of rat vas deferens by cyclic AMP analogs. Mol Pharmacol. 1991;39:233-238.

29. Castigli E, Wilson SA, Scott S, et al. TACI and BAFF-R mediate isotype switching in B cells. J Exp Med. 2005;201:35-39.
30. Planelles L, Carvalho-Pinto CE, Hardenberg G, et al. APRIL promotes B-1 cell-associated neoplasm. Cancer Cell. 2004;6:399-408.
31. Fagarasan S, Kinoshita K, Muramatsu M, Ikuta K, Honjo T. In situ class switching and differentiation to IgA-producing cells in the gut lamina propria. Nature. 2001;413:639-643.
32. Fagarasan S, Honjo T. Intestinal IgA synthesis: regulation of front-line body defences. Nat Rev Immunol. 2003;3:63-72.
33. Sasisekharan R, Shriver Z, Venkataraman G, Narayanasami U. Roles of heparan-sulfate glycosaminoglycans in cancer. Nat Rev Cancer. 2002;2:521-528.
34. Ng LG, Sutherland AP, Newton R, et al. B cell-activating factor belonging to the TNF family (BAFF)-R is the principal BAFF receptor facilitating BAFF costimulation of circulating T and B cells. J Immunol. 2004;173:807-817.
35. Bossen C, Ingold K, Tardivel A, et al. Interactions of tumor necrosis factor (TNF) and TNF receptor family members in the mouse and human. J Biol Chem. 2006;281:13964-13971.
36. Fagarasan S, Honjo T. T-independent immune response: new aspects of B cell biology. Science. 2000;290:89-92.
37. Martin F, Oliver AM, Kearney JF. Marginal zone and B1 B cells unite in the early response against T-independent blood-borne particulate antigens. Immunity. 2001;14:617-629.
38. Macpherson AJ, Lamarre A, McCoy K, et al. IgA production without mu or delta chain expression in developing B cells. Nat Immunol. 2001;2:625-631.
39. MacLennan I, Vinuesa C. Dendritic cells, BAFF, and APRIL: innate players in adaptive antibody responses. Immunity. 2002;17:235-238.

Noninvasive and real-time assessment of reconstructed functional human endometrium in NOD/SCID/γ_c^{null} immunodeficient mice

Hirotaka Masuda*†, Tetsuo Maruyama*‡, Emi Hiratsu†, Junichi Yamane†§, Akio Iwanami†§, Takashi Nagashima*, Masanori Ono*, Hiroyuki Miyoshi¶, Hirotaka James Okano†‖, Mamoru Ito**, Norikazu Tamaoki**, Tatsuji Nomura**, Hideyuki Okano†‖, Yumi Matsuzaki†‖, and Yasunori Yoshimura*

Departments of *Obstetrics and Gynecology, †Physiology, and §Orthopedic Surgery, Keio University School of Medicine, Tokyo 160-8582, Japan; ¶Subteam for Manipulation of Cell Fate, BioResource Center, RIKEN Tsukuba Institute, Ibaraki 305-0074, Japan; Core Research for Evolutional Science and Technology (CREST), Japan Science and Technology Agency, Saitama 332-0012, Japan; and **Central Institute for Experimental Animals, Kanagawa 216-0001, Japan

Edited by R. Michael Roberts, University of Missouri, Columbia, MO, and approved December 12, 2006 (received for review May 24, 2006)

Human uterine endometrium exhibits unique properties of cyclical regeneration and remodeling throughout reproductive life and also is subject to endometriosis through ectopic implantation of retrogradely shed endometrial fragments during menstruation. Here we show that functional endometrium can be regenerated from singly dispersed human endometrial cells transplanted beneath the kidney capsule of NOD/SCID/γ_c^{null} immunodeficient mice. In addition to the endometrium-like structure, hormone-dependent changes, including proliferation, differentiation, and tissue breakdown and shedding (menstruation), can be reproduced in the reconstructed endometrium, the blood to which is supplied predominantly by human vessels invading into the mouse kidney parenchyma. Furthermore, the hormone-dependent behavior of the endometrium regenerated from lentivirally engineered endometrial cells expressing a variant luciferase can be assessed noninvasively and quantitatively by *in vivo* bioluminescence imaging. These results indicate that singly dispersed endometrial cells have potential applications for tissue reconstitution, angiogenesis, and human–mouse chimeric vessel formation, providing implications for mechanisms underlying the physiological endometrial regeneration during the menstrual cycle and the establishment of endometriotic lesions. This animal system can be applied as the unique model of endometriosis or for other various types of neoplastic diseases with the capacity of noninvasive and real-time evaluation of the effect of therapeutic agents and gene targeting when the relevant cells are transplanted beneath the kidney capsule.

animal model | bioluminescence imaging | endometriosis | menstruation | angiogenesis

Human endometrium lines the uterus and comprises luminal and glandular epithelial cells, stromal fibroblasts, vascular smooth muscle cells, endothelial cells, and immune competent cells. These cell components coordinately participate in the cyclical changes of human endometrium, including proliferation, differentiation, and tissue breakdown and shedding under the influence of estrogen and progesterone during the menstrual cycle. This unique system of cyclic tissue regeneration also depends on the cyclical growth and regression of the blood vessels that supply the endometrium (1). In addition, angiogenesis is deeply involved in the pathogenesis of endometrium-derived disorders such as endometriosis (2). Endometriosis, one of the most common gynecological diseases, is characterized by the presence of functional endometrial-like tissue outside the uterine cavity. It is an estrogen-dependent disorder associated with substantial morbidity; however, the etiology and pathophysiology are not well elucidated (3). To study the physiology of normal endometrium and the pathogenesis of endometriosis, a variety of *in vivo* models using small animals has been developed by using the transplantation of autologous or heterologous endometrial cells tissues or endometriotic tissues (4).

In the present study, taking advantage of newly developed severe immunodeficient mice, NOD/SCID/γ_c^{null} (NOG) mice (5), we have developed a mouse model that satisfies the following requirements: (*i*) the transplant of human origin is quantitatively and characteristically uniform in each animal, (*ii*) functional and morphological changes characteristic of human eutopic and/or ectopic endometrium are reproduced, and (*iii*) the transplant is assessable for a long term in a noninvasive, real-time, and quantitative manner. By using this model, evidence has been obtained suggesting a previously uncharacterized mechanism underlying the regeneration and remodeling of human endometrium and the pathogenesis of endometriosis.

Results

Reconstruction of Human Endometrial Tissues in NOG Mice. We first isolated and dissociated endometrial cells mechanically and enzymatically from human cycling endometrium. We transplanted 5×10^5 of these singly dispersed endometrial cells (SDECs) beneath each kidney capsule of ovariectomized (OVX)-NOG mice. Multiple immunological dysfunctions, including cytokine production incapacity and functional incompetence of T, B, and natural killer (NK) cells, may explain the high success rates of xenografts in NOG mice (5). Xenotransplanted NOG mice were subjected to different hormonal treatments (Fig. 1*A*).

Surprisingly, endometrium-like tissues were found in all of the transplanted kidneys of NOG mice ($n = 30$) hormonally treated for 10 weeks (Fig. 1*B*), whereas a very tiny but macroscopically identifiable tissue was reconstituted in only 1 of 12 nonhormonally treated mice (data not shown). Treatment with estradiol (E_2) and progesterone (P_4), or $E_2 + P_4$ treatment, generated a large

Author contributions: H. Masuda, T.M., H.O., Y.M., and Y.Y. designed research; H. Masuda, T.M., E.H., J.Y., A.I., T. Nagashima, and M.O. performed research; H. Miyoshi, H.J.O., M.I., N.T., and T. Nomura contributed new reagents/analytic tools; H. Masuda and T.M. analyzed data; and H. Masuda, T.M., H.O., Y.M., and Y.Y. wrote the paper.

The authors declare no conflict of interest.

This article is a PNAS direct submission.

Abbreviations: NOG, NOD/SCID/γ_c^{null}; SDECs, singly dispersed endometrial cells; OVX, ovariectomized; NK, natural killer; E_2, estradiol; P_4, progesterone; $E_2 + P_4$, treatment with E_2 and P_4; Vm, vimentin; αSMA, α smooth muscle actin; PR, P_4 receptor; PRL, prolactin; BLI, bioluminescence imaging; YFP, yellow fluorescent protein; CBR luc, click beetle red-emitting luciferase; PI, propidium iodide.

‖To whom correspondence should be addressed at: Department of Obstetrics and Gynecology, Keio University School of Medicine, 35 Shinanomachi, Shinjuku-ku, Tokyo 160-8582, Japan. E-mail: tetsuo@sc.itc.keio.ac.jp.

This article contains supporting information online at www.pnas.org/cgi/content/full/0604310104/DC1.

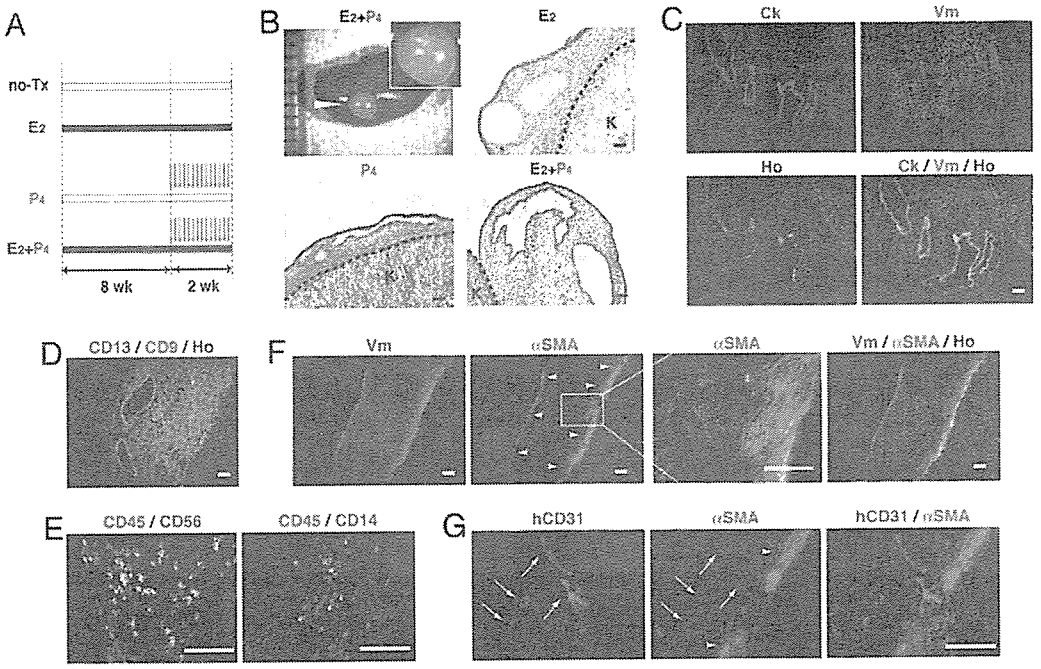

Fig. 1. Reconstruction of human endometrium-like tissue from SDECs. (*A*) Experimental design and hormonal treatment. NOG mice were OVX, xenotransplanted with SDECs, and then treated without (no-Tx) or with s.c. implantation of usually two E_2 pellets alone (E_2) or with a daily s.c. injection of P_4 (red arrows) for the last 2 weeks (P_4) or in combination with E_2 (E_2 + P_4); they were finally nephrectomized 10 weeks after transplantation. (*B*) Macroscopic and microscopic findings of the transplanted site (arrowhead) of NOG mice 10 weeks after xenotransplantation. H&E staining was performed on the transplanted lesion of NOG mice treated with E_2, P_4, or E_2 + P_4 as indicated. The borders between the reconstituted tissue and the mouse kidney (K) are indicated by the dotted lines. (*C–G*) Immunofluorescence staining of the endometrial reconstructs in the E_2 + P_4-treated NOG mice by using antibodies against cytokeratin (Ck) and Vm (*C*), CD13 and CD9 (*D*), CD56 or CD14 in combination with CD45 (*E*), Vm and α-SMA (*F*), or human CD31 (hCD31) and α-SMA (*G*), followed by Hoechst (Ho) staining. (*F*) Arrows point to the regions prominently immunoreactive for α-SMA. A small box marks a region shown at higher magnification in the adjacent panel as indicated (*G*). Arrows and arrowheads indicate hCD31$^+$/α-SMA$^-$ cells and hCD31$^-$/α-SMA$^+$ cells, respectively. (Scale bars: 100 μm.)

cystic mass (Fig. 1*B*, arrowhead) with a fine surface vasculature (Fig. 1*B Inset*). Hematoxylin and eosin (H&E) staining demonstrated that well delineated glands and stroma were present in the transplanted lesions dissected from E_2- or E_2 + P_4-treated mice (Fig. 1*B*). Furthermore, the growth of the endometrial transplants together with the enlargement of the uterus were E_2 dose-dependent [supporting information (SI) Fig. 6].

Immunofluorescence studies revealed that the reconstructed tissues, but not the mouse kidney, were stained exclusively with anti-human vimentin (Vm) antibody (clone V9) (Fig. 1*C*). As V9 can recognize only human Vm, the reconstructed tissue was clearly of human origin. In addition, the stroma was positive for CD10 (data not shown) and CD13, both endometrial stromal cell markers (6), whereas the glandular structure was positive for cytokeratin and CD9, both epithelial markers (6) (Fig. 1 *C* and *D*). Human endometrial tissue and decidualized endometrium in pregnancy contain large numbers of CD45-positive leukocytes, the vast majority of which are CD56$^+$ NK cells with the other populations being CD14$^+$ macrophages and T cells (7). In agreement with this profile, CD45$^+$ cells were abundant in the reconstructed tissue, and the proportions of CD56$^+$ and CD14$^+$ cells, both of human origin, were similar to those in the eutopic endometrium (Fig. 1*E*).

Expression of α-smooth muscle actin (αSMA) is ubiquitously prominent in the uterine myometrium but is mainly confined to vascular smooth muscle cells in the endometrium (8). In the Vm-positive regenerated tissue, αSMA antibody preferentially and potently reacted with two distinct regions: one adjacent to the mouse kidney parenchyma and the other beneath the serous membrane (Fig. 1*F*, arrowheads). These two regions mainly consist of αSMA-positive spindle-shaped fibroblastic cells morphologically similar to myometrial cells (Fig. 1*G*). The vast majority of these densely populated αSMA$^+$ cells did not colocalize with CD31$^+$ endothelial cells (Fig. 1*G*, arrowheads). In the same area, however, some αSMA$^+$ cells were present along with cells positive for CD31, an endothelial cell marker (Fig. 1*G*, arrows). These results collectively suggest that some, but not most, αSMA$^+$ cells contribute to the formation of the vessels, presumably as pericytes. Thus, the reconstituted tissue possessed hierarchical architecture distinctly composed of endometrium- and myometrium-like layers (Fig. 1*G*), closely resembling the normal uterine structure at the interface between endometrium and myometrium. Absence of αSMA$^+$ cells in SDECs (data not shown) indicated that they did not contain differentiated myometrial cells, which may account for the lack of spiral arterioles in the reconstituted endometrial tissues, because spiral arteries arise from the myometrium. Furthermore, given the potential of endometrial stroma for differentiation into smooth muscle (9), it is likely that the generation of myometrial-like components may be caused by the transdifferentiation of SDECs into smooth muscle cells. Alternatively, it also remains possible that SEDCs include a population of undifferentiated smooth muscle precursor cells. Taken together, SDECs have the potential to regenerate the endometrium ectopically with tissue polarity, glandular structures, and endometrial cell components.

Neovascularization of the Reconstructed Endometrium by Human–Mouse Chimeric Vessels. We further investigated the vascular components of the E_2 + P_4-exposed endometrial reconstruct. As shown in Fig. 2 *A*, human CD31$^+$ (arrows) or mouse CD31$^+$ (arrowheads) endothelial cells coexisted abundantly in the reconstructed tissue in E_2 + P_4-treated NOG mice; however, they did not appear to anastomose with each other (Fig. 2*A Right*).

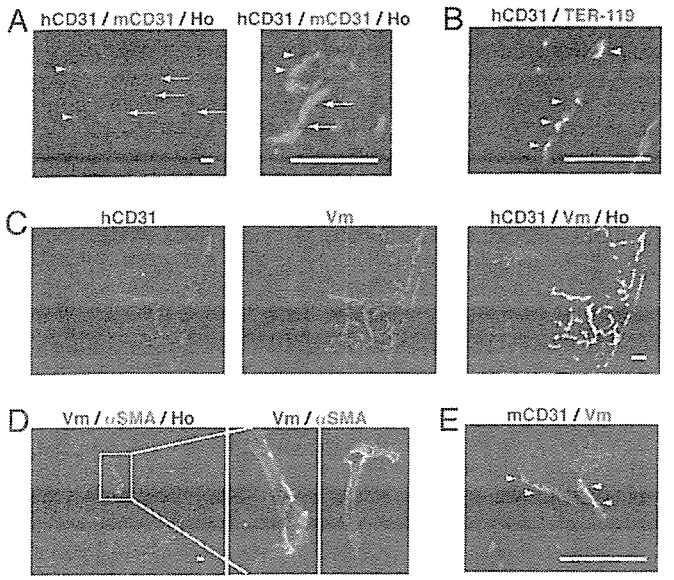

Fig. 2. Vascularization of the reconstructed endometrium predominantly composed of human–mouse chimeric vessels. Immunofluorescence staining of the reconstituted endometrial tissue (*A*) and the mouse kidney parenchyma adjacent to the reconstituted tissue (*B–E*) in the E_2 P_4-treated NOG mice by using antibodies against human CD31 (hCD31) and murine CD31 (mCD31) (*A*), hCD31 and TER-119 (*B*), hCD31 and Vm (*C*), Vm and αSMA (*D*), or mCD31 and Vm (*E*), followed by Hoechst (Ho) staining. (*A*) Arrows and arrowheads indicate hCD31 cells and mCD31 cells, respectively. (*B*) Arrowheads show hCD31 vessels containing mouse erythrocytes positive for TER-119. (*D*) A small box marks a region shown at higher magnification in the adjacent panel as indicated. (*E*) Arrowheads point to mCD31 vessels that were present together with human Vm cells. (Scale bars: 100 μm.)

Intriguingly, cells positive for TER-119, a mouse erythrocyte marker, were found not only in the mouse CD31 vessels (SI Fig. 7) but also in the vessels consisting of human $CD31^+$ endothelial cells (Fig. 2*B*, arrowheads), indicating that the human-originated vasculature functioned as a circulation system in the reconstructed endometrium.

To address the presence of chimeric vessels composed of human and mouse endothelial cells, we performed histological analyses focusing on the mouse kidney adjacent to the reconstituted endometrium. We found that human-originated (human Vm-positive) cells migrated into the mouse kidney parenchyma and most were positive for human CD31 (Fig. 2*C*). The anti-αSMA antibody reacts with both mouse and human smooth muscle cells. Therefore, as most Vm^+ cells also are positive for human CD31, $\alpha SMA^-/Vm^+$ cells (Fig. 2*D*, green) corresponded to human $CD31^+$ cells in the mouse kidney parenchyma, whereas $\alpha SMA^+/Vm^-$ cells (Fig. 2*D*, red) were mouse smooth muscle cells. Thus, there existed chimeric vessels of two distinct species in the mouse kidney parenchyma (Fig. 2*D Center* and *Right*), which was confirmed by the colocalization of murine $CD31^+$ endothelial cells and human Vm-positive cells (Fig. 2*E*, arrowheads).

Hormone-Dependent Changes of the Reconstructed Endometrium. It is well known that the endometrial P_4 receptor (PR) is up-regulated by E_2 exposure. In agreement, PR was expressed prominently in the E_2-exposed reconstruct (Fig. 3*A*). In addition, glandular cells became pseudostratified (Fig. 3*A*, arrowheads), reflecting a high level of E_2-dependent proliferation activity.

Decidualization is the P_4-induced differentiation of E_2-primed endometrial stromal cells, which occurs during the P_4-dominated secretory phase and pregnancy. Decidualized stromal cells become enlarged and round, and they produce many bioactive substances, including prolactin (PRL) (10). Accordingly, PRL was expressed prominently in the stromal cells, but not glandular cells, of $E_2 + P_4$-exposed endometrial reconstructs (Fig. 3*B*), indicating the successful spatiotemporal induction of PRL in this animal model. In addition to the strong staining of PRL caused by relatively high levels of P_4, H&E staining revealed edematous stroma with predecidual changes, accumulation of mononuclear leukocytes beneath the glandular epithelium, and tortuous glands (SI Fig. 8), all of which are distinctive morphological changes of secretory-phase endometrium.

One of the unique events of human cycling endometrium is the breakdown and shedding of tissue, i.e., menstruation, which is induced by the withdrawal of P_4. To provoke menstrual changes in the reconstructed endometrium, OVX-NOG mice were subjected to cyclic treatment with $E_2 + P_4$ (cyclic $E_2 + P_4$) after xenotransplantation and thereafter to P_4 withdrawal (Fig. 3*C*). Grafts collected a week after the second P_4 withdrawal contained large blood-filled cysts that were similar to red spot lesions (Fig. 3*D*, arrowheads) typical of aggressive endometriosis (11). H&E and immunofluorescence staining of the cystic lesion revealed that the glandular structures partly were destroyed (Fig. 3*E*, arrowheads) and that hemorrhage had occurred in the degenerative stroma (Fig. 3*E*, arrow).

Lentiviral Introduction of Reporter Genes into Primary Endometrial Cells. Bioluminescence imaging (BLI) recently has emerged as a useful tool for tumor, hematopoietic, and neural cell tracking

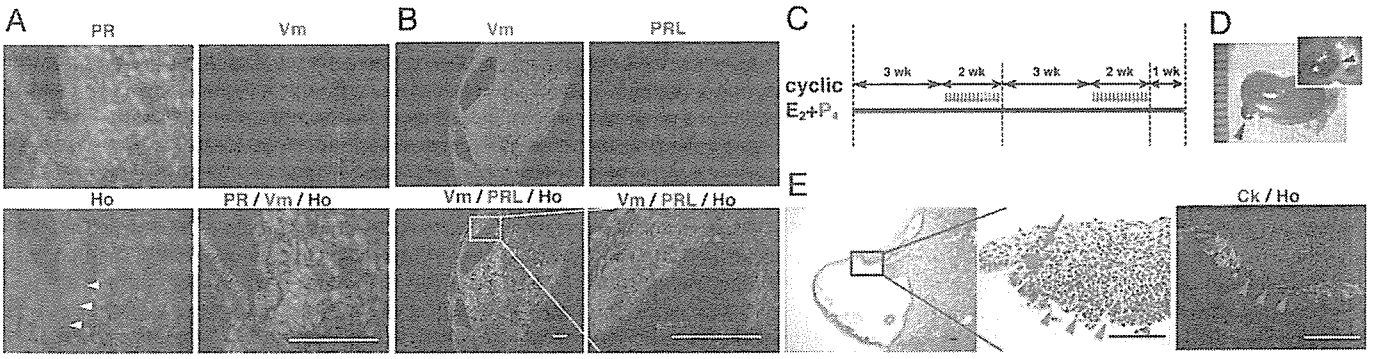

Fig. 3. Hormone-dependent morphological and functional changes of the reconstructed endometrium. Immunofluorescence staining of the reconstituted endometrial tissues in the E_2-treated (*A*) or E_2 P_4-treated (*B*) NOG mice by using antibodies against PR and Vm (*A*) and Vm and PRL (*B*), followed by Hoechst (Ho) staining. (*A*) Arrowheads show pseudostratified glandular cells. (*C*) Hormonal treatment protocol (cyclic E_2 P_4) for induction of menstruation-like tissue breakdown and shedding. (*D*) Macroscopic findings of the transplanted site (arrows) of a NOG mouse treated with cyclic E_2 P_4. (*E*) H&E and immunofluorescence staining of the transplanted lesion in the cyclic E_2 P_4-treated mice. The glandular structure was partially disrupted (arrowheads), and hemorrhage occurred in the stroma (arrow). (*B* and *E*) A small box marks a region shown at higher magnification in the adjacent panel as indicated. (Scale bars: 100 μm.)

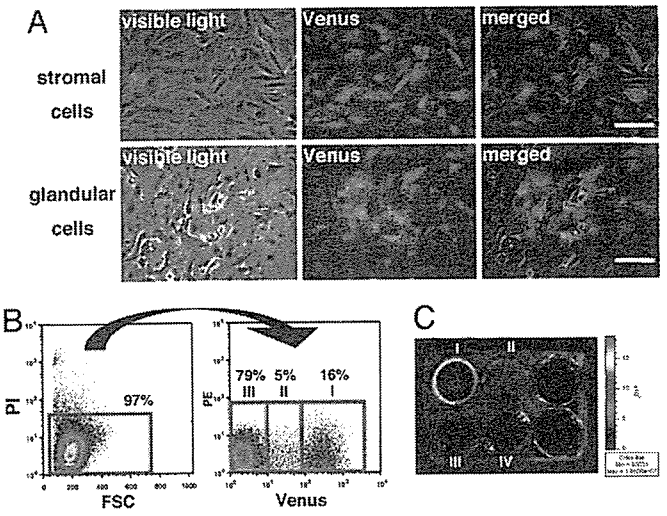

Fig. 4. Expression of both fluorescence and luminescence markers in the lentivirally transduced SDECs. (*A*) Phase-contrast and fluorescence microscopy of the primary cultures of lentivirally transduced endometrial stromal (*Upper*) and glandular (*Lower*) cells. (*B*) A representative flow cytometric profile of the PI-negative fraction (red box at *Left*) of the lentivirally transduced SDECs consisting of three subpopulations (*Right*) based on the fluorescence intensity: high (I), low (II), and negative (III) subpopulations. (*C*) Macroscopic luminescence image of a six-well dish where each subpopulation, as sorted in *B*, was cultured in the corresponding well. Noninfected SDECs were cultured in the "IV" well.

studies in living animals (12–15). To apply this animal model to the BLI system, we have developed a recombinant lentivirus capable of introducing and stably expressing both the Venus [a yellow fluorescent protein (YFP) mutant] (16) gene and the click beetle red-emitting luciferase (CBR luc, a luciferase variant) (17) gene in the primary culture endometrial cells. These two reporter markers are useful for cell sorting and the detection of living cells from outside the body.

Fluorescence microscopy revealed YFP signals were detected in ≈20–60% of the primary culture SDECs infected with the recombinant lentivirus (Fig. 4*A*). To quantitatively assess YFP intensity, these SDECs were harvested and stained with propidium iodide (PI). Then, PI-negative SDECs were sorted by flow cytometry and further divided into three groups based on YFP intensity: high (I), low (II), and negative (III) (Fig. 4*B*). These three subpopulations and noninfected SDECs (IV) were plated onto the corresponding wells of a six-well dish, cultured, and subjected to BLI (Fig. 4*C*). BLI revealed the luminescence intensity to correlate well with the YFP intensity (Fig. 4*C*).

Noninvasive and Quantitative Assessment of the Reconstituted Endometrium by BLI. The OVX-NOG mice were transplanted with the lentivirally engineered SDECs expressing CBR luc beneath the kidney capsule, simultaneously implanted with two E_2 pellets, and subjected to BLI analysis 8 weeks after xenotransplantation. BLI of the ventrally positioned NOG mouse revealed bioluminescence signals in locations corresponding to the bilateral kidney (Fig. 5*A Upper*). To confirm that these signals did indeed originate from the transplanted kidney, a dorsally positioned laparotomized mouse (Fig. 5*A Lower Left*) and its excised kidneys (Fig. 5*A Lower Right*) were subjected to BLI, which clearly indicated that the intense focal bioluminescent spots were confined to the transplanted sites.

To determine whether the growth behavior of the reconstructed tissue can be assessed quantitatively and sequentially, we treated the xenotransplanted OVX-NOG mice without or with one or two E_2 pellets. Sequential BLI of the mice at 3–9 weeks after xenotransplantation revealed that the signal intensities reflecting the volume of the reconstructed tissue were enhanced in an E_2 dose- and time-dependent manner (Fig. 5*B*), in agreement with the macroscopic findings (SI Fig. 6). In contrast, the signal intensity was kept low and constant or rather decreased in nonhormonally treated mice (Fig. 5*B*).

To validate our BLI system as a tool for drug testing, we measured the bioluminescence signals in xenotransplanted OVX-NOG mice treated with E_2 in combination with ICI 182,780 (Tocris Cookson Inc., Ellisville, MO), a pure estrogen antagonist. In contrast to the mice treated with E_2 alone (Fig. 5*B*), the signal intensity was decreased 2–3 months after the cotreatment with E_2 and ICI 182,780 (Fig. 5*C*), indicating that the antagonistic effect of ICI 182,780 can be assessed noninvasively.

Finally, we monitored the dynamic changes of the endometrial reconstructs during an artificial menstrual cycle induced by cyclic $E_2 + P_4$ treatment (Fig. 5*D*). Sequential BLI revealed that the signal intensities fluctuated dramatically in accord with the addition and withdrawal of P_4 (Fig. 5*D*), indicating that the decrease and reincrease in signal intensity faithfully reflected tissue breakdown and regression after P_4 withdrawal as shown in Fig. 3 *C* and *D* and, presumably, subsequent tissue regeneration, respectively (Fig. 5*D*). Thus, the repeated menstrual cycle-related changes of the transplants can be noninvasively monitored in living NOG mice.

Discussion

Human endometrium is believed to regenerate from the lower basalis layer, a germinal compartment that persists after menstruation, to give rise to a new functionalis layer (18). The potential of singly dissociated endometrial cells to reconstitute the endometrial tissue raises a possibility that endometrial stem/progenitor cells present in the functionalis layer also may participate in the physiological regeneration of the endometrium through their recycle and reuse. Our hypothesis seems to be supported by the recent report that label-retaining cells, which are thought to be tissue stem/progenitor cells, are present not only at the endometrial–myometrial junction but also in luminal epithelium and stroma adjacent to luminal epithelium and near blood vessels in mice (19).

Several experiments in which human endometrial tissues were transplanted into immunodeficient mice such as SCID and nude mice have shown that endometriotic lesions derive their blood supply from the surrounding vascular network (20–22). Furthermore, native human-originated graft vessels disappear gradually, but host vessels instead invade during revascularization of endometrial explants (21–24). As NK cells play a critical role in the IL-12-mediated inhibition of angiogenesis (25), the lack of human endometrial graft-originated vessels in SCID and nude mice in previous studies (20–24) may be attributable to the presence of functioning NK cells, which would attack various immature precursor cells that show low MHC expression level (26). In contrast, we demonstrate here that human-derived vessels are abundant in the endometrial reconstructs, and that they invade into the mouse kidney parenchyma and become connected with mouse vessels functioning as a circulation system. Because NK cells are functionally incompetent in the NOG mouse (5), the human-originated neovascularization is allowed to take place. Given that impaired NK cell cytotoxicity contributes to inadequate removal of ectopic endometrial cells from the peritoneal cavity (27), this endometriosis model using NOG mice may be suitable for the study of the pathogenesis of endometriosis.

Our findings raise the possibility that endothelial cells or their progenitors derived from human endometrium may have a unique angiogenic potential to migrate, invade, and form the vasculature in host tissue, even when originating from a different species. Bussolati *et al.* (28) have reported that tumor-derived endothelial cells, but not normal endothelial cells, possess a unique neoangiogenic ability to grow in immunodeficient mice and to form vascular structures linked with the mouse circulation. It therefore is conceivable that, in addition to the peritoneal environment (29), the

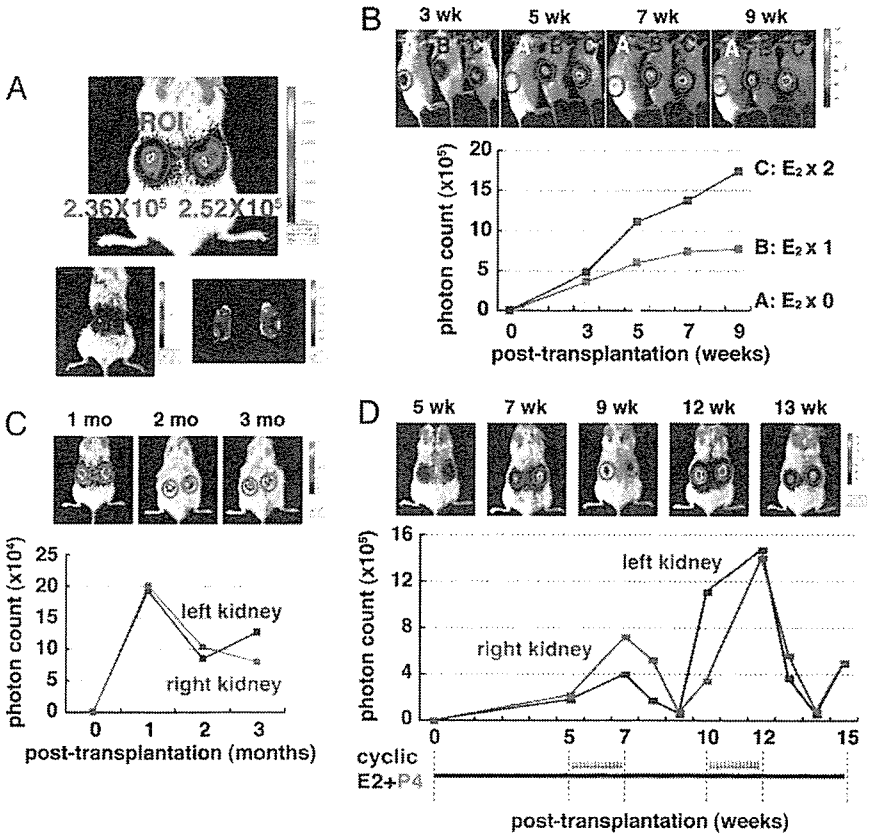

Fig. 5 Optical bioluminescence images and noninvasive quantitative assessment of the endometrial tissues reconstructed from lentivirally transduced SDECs in living NOG mice. (*A*) A bioluminescence image of the endometrial reconstructs expressing CBR luc in a ventrally positioned NOG mouse treated with E_2 alone. Bioluminescence images of the laparotomized mouse at the dorsal position (*Lower Left*) and its excised kidneys (*Lower Right*). (*B–D*) Representative BLI (*Upper*) and serial photon count measurements (*Lower*) of xenotransplanted OVX-NOG mice treated for different durations with the various indicated doses of E_2 pellets (*B*), with E_2 in combination with daily injections of ICI 182,780 (*C*), or with cyclic E_2 + P_4 treatment to induce artificial menstrual cycle-related changes (*D*) in accordance with a similar protocol as shown in Fig. 3C

angiogenic potential of the endometrial endothelial cells per se may be one of the critical determinants for the establishment and development of the endometriotic lesion. Antiangiogenic therapy recently has been proposed as an alternative treatment for endometriosis (23, 30). This therapeutic strategy might be strengthened further by targeting endometrium- or endometriosis-specific angiogenesis, as postulated here.

The animal model described here has several advantages over the endometriosis models in current use. First, a single-cell suspension is adequate for several experimental procedures such as cell selection, genetic engineering, and quantitative assessment, as compared with the dissected sections of endometrial or endometriotic tissues used for the transplants in many endometriosis models (4). The use of SDECs also allows relatively easy production of several or even dozens of homogeneous mice, because only a small number of endometrial cells is required for the reconstruction of the endometrium. Second, the regenerated tissues exhibit abundant vascularization and the preservation of endometrial cell components and tissue organization, which enable the long-term maintenance of the reconstructed structure and the hormone-dependent changes characteristic of human cycling endometrium and/or endometriotic explants. Third, taking advantage of the lentivirus and CBR luc, whose emitted light has the capacity to pass through the thickened tissue, the transplants can be assessed for a prolonged period in a noninvasive, real-time, and quantitative manner.

Thus, it is demonstrated here that SDECs have the capacity for tissue regeneration and reconstruction. Combining this unique potential together with NOG mice and lentivirus-mediated cell engineering, we report the unique animal model suitable for the study of endometrial physiology/pathophysiology and the pathogenesis of endometriosis through noninvasive, real-time, and quantitative assessment of ectopically reconstituted endometrium-like tissues. Furthermore, this animal model system can be potentially applicable for drug testing and gene-target validation not only in endometriosis but also in other various types of neoplastic disease when the relevant primary culture cells or cell lines are transplanted beneath the kidney capsule.

Materials and Methods

Detailed protocols can be found in *SI Methods*.

Tissue Collection. Proliferative phase endometrial specimens (n = 20) without any abnormalities or malignancies were collected from consenting women (aged 39–51 years) with normal menstrual cycles undergoing total abdominal hysterectomy for benign gynecological diseases. The use of these human specimens was approved by the Keio University Ethics Committee.

Preparation of SDECs. Human endometrial specimens were dissociated mechanically and enzymatically, filtrated, isolated by Ficoll gradient, and finally separated into endometrial stromal and glandular epithelial cell fractions as described previously (31, 32), with certain modifications. In brief, endometrial tissue samples were cut into small pieces and digested with 0.2% (wt/vol) collagenase (Wako, Osaka, Japan) and 0.05% DNase I

(GIBCO, Carlsbad, CA) in DMEM for 1.5 h at 37°C on a shaking rotor. The tissue digest was filtrated through a sterile 407-μm mesh filter, followed by a 40-μm cell strainer (BD Biosciences, Bedford, MA). The glandular fragments retained in the strainer were recovered by back-flushing.

Stromal cell suspension was layered over Ficoll-Paque PLUS (Amersham Biosciences, Piscataway, NJ) and centrifuged to remove red blood cells. The media/Ficoll interface layer mainly containing stromal and immune cells was aspirated and washed. Glandular fragments were digested with 0.05% trypsin-EDTA solution (Sigma–Aldrich, St. Louis, MO) and 0.05% DNase I by pipetting, washed, and filtrated through a 40-μm cell strainer to yield a single-cell suspension. Mixtures of these two fractions were designated SDECs and were used as transplants or subjected to cell culture and lentiviral infection. Flow cytometric analysis revealed that the percentages (mean ± SD) of CD9, CD13, CD31, and CD45 were 12.0 ± 7.2%, 40.2 ± 9.5%, 2.4 ± 1.0%, and 46 ± 13.0% in SDECs, respectively. Procedures for preparing SDECs and the representative flow cytometric data are summarized schematically in SI Fig. 9.

Xenotransplantation and Hormonal Treatment. NOG mice (5) were used for xenotransplantation experiments. The single-cell suspension of SDECs (5×10^5) in 5–10 μl of DMEM was injected underneath the kidney capsules (for details see *SI Methods*). At transplantation, NOG mice were OVX and implanted s.c. without (Fig. 1*A*, "no-Tx") or with one or usually two E_2 pellets (Fig. 1*A*, "E_2") (1.5 mg of E_2 per pellet; Innovative Research of America, Sarasota, FL). For P_4 or $E_2 + P_4$ treatment, 1 mg of P_4 was injected s.c. every day for the last 2 weeks (Fig. 1*A*). For cyclic $E_2 + P_4$ treatment, xenotransplanted OVX-NOG mice implanted with two E_2 pellets were subjected to two cycles of daily P_4 injections for 2 weeks with a 3-week interval (Figs. 3*D* and 5*D*). In some mice implanted with an E_2 pellet, 100 μg per body weight per day of ICI 182,780 was injected s.c. every day from the first day of transplantation (Fig. 5*C*). These xenotransplanted mice were nephrectomized according to the experimental protocol (for details see *SI Methods*).

Histological and Immunofluorescence Analysis. Serial cryosections of the kidneys excised from the xenotransplanted NOG mice were air-dried, washed, and fixed. After permeabilization and blocking, tissue sections were incubated with the pretitrated primary antibodies listed in SI Table 1. For indirect fluorescence staining, the first antibodies were visualized by incubation with secondary antibodies conjugated with Alexa Fluor 488 (green) or 568 (red) (Molecular Probes, Eugene, OR). Nuclei were stained with Hoechst 33258. Images were collected as described in *SI Methods*.

Infection of Lentivirus Expressing CBR luc and Preparation of Transduced SDECs. The gene fragment of CBR luc was excised from the pCBR-Basic vector (Promega, Madison, WI) and cloned into pCSII-EF-MCS-IRES2-Venus (33). Viral stock was produced as described in ref. 15. SDECs were cultured, infected with lentivirus, continuously propagated, harvested, and then dissociated into single cells. The PI-negative/Venus-positive SDECs were sorted by a MoFlo (Cytomation, Fort Collins, CO) and plated onto a culture dish or transplanted beneath the kidney capsule on the dorsal side in OVX-NOG mice.

BLI. We used a Xenogen-IVIS 100 cooled CCD optical macroscopic imaging system (SC BioScience Corporation, Tokyo, Japan) for BLI. For *in vitro* imaging, SDECs were plated at equal density and imaged in the presence of 150 μg/ml D-luciferin (SC BioScience Corporation). For *in vivo* imaging, OVX-NOG mice xenotransplanted with lentivirally engineered SDECs were anesthetized and given an i.p. injection of D-luciferin (150 mg/kg body weight). All images were analyzed as described in *SI Methods*. To quantify the measured light, regions of interest (ROI) were defined over the transplanted area and all values were examined from an equal ROI.

We thank Tetsuro Tamaki for advice on xenotransplantation; members of the T.M. laboratory, members of the Kamakura Research Laboratories (Chugai Pharmaceutical Co., Ltd.), and Lawrence Y. Lein for technical assistance and helpful advice; and Shoka Kan, Kiyoshi Amemiya, and Yurie Yamamoto for collecting endometrial samples. This study was supported, in part, by grant-in-aids from the Japan Society for the Promotion of Science (to T.M. and to Y.Y.), a national grant-in-aid for the establishment of a high-tech research center in a private university (to T.M.), and a grant-in-aid from the 21st Century Center of Excellence program of the Ministry of Education, Science, and Culture of Japan at Keio University. H. Masuda is a recipient of research fellowships of the Japan Society for the Promotion of Science for Young Scientists.

1. Smith SK (2001) *Trends Endocrinol Metab* 12:147–151.
2. Donnez J, Smoes P, Gillerot S, Casanas-Roux F, Nisolle M (1998) *Hum Reprod* 13:1686–1690.
3. Giudice LC, Kao LC (2004) *Lancet* 364:1789–1799.
4. Grummer R (2006) *Hum Reprod Update* 12:641–649.
5. Ito M, Hiramatsu H, Kobayashi K, Suzue K, Kawahata M, Hioki K, Ueyama Y, Koyanagi Y, Sugamura K, Tsuji K, *et al.* (2002) *Blood* 100:3175–3182.
6. Fujiwara H, Tatsumi K, Kosaka K, Sato Y, Higuchi T, Yoshioka S, Maeda M, Ueda M, Fujii S (2003) *J Clin Endocrinol Metab* 88:3437–3443.
7. Vince GS, Johnson PM (2000) *Biochem Soc Trans* 28:191–195.
8. Kohnen G, Campbell S, Jeffers MD, Cameron IT (2000) *Hum Reprod* 15:284–292.
9. Bird CC, Willis RA (1965) *J Pathol Bacteriol* 90:75–81.
10. Dunn CL, Kelly RW, Critchley HO (2003) *Reprod Biomed Online* 7:151–161.
11. Nisolle M, Donnez J (1997) *Fertil Steril* 68:585–596.
12. Contag CH, Bachmann MH (2002) *Annu Rev Biomed Eng* 4:235–260.
13. Wang X, Rosol M, Ge S, Peterson D, McNamara G, Pollack H, Kohn DB, Nelson MD, Crooks GM (2003) *Blood* 102:3478–3482.
14. Sweeney TJ, Mailander V, Tucker AA, Olomu AB, Zhang W, Cao Y, Negrin RS, Contag CH (1999) *Proc Natl Acad Sci USA* 96:12044–12049.
15. Okada S, Ishii K, Yamane J, Iwanami A, Ikegami T, Katoh H, Iwamoto Y, Nakamura M, Miyoshi H, Okano HJ, *et al.* (2005) *FASEB J* 19:1839–1841.
16. Nagai T, Ibata K, Park ES, Kubota M, Mikoshiba K, Miyawaki A (2002) *Nat Biotechnol* 20:87–90.
17. Zhao H, Doyle TC, Coquoz O, Kalish F, Rice BW, Contag CH (2005) *J Biomed Opt* 10:41210.
18. Padykula HA (1991) *Ann NY Acad Sci* 622:47–56.
19. Chan RW, Gargett CE (2006) *Stem Cells* 24:1529–1538.
20. Nisolle M, Casanas-Roux F, Donnez J (2000) *Fertil Steril* 74:306–312.
21. Grummer R, Schwarzer F, Bainczyk K, Hess-Stumpp H, Regidor PA, Schindler AE, Winterhager E (2001) *Hum Reprod* 16:1736–1743.
22. Bruner-Tran KL, Webster-Clair D, Osteen KG (2002) *Ann NY Acad Sci* 955:328–339.
23. Hull ML, Charnock-Jones DS, Chan CL, Bruner-Tran KL, Osteen KG, Tom BD, Fan TP, Smith SK (2003) *J Clin Endocrinol Metab* 88:2889–2899.
24. Eggermont J, Donnez J, Casanas-Roux F, Scholtes H, Van Langendonckt A (2005) *Fertil Steril* 84:492–499.
25. Yao L, Sgadari C, Furuke K, Bloom ET, Teruya-Feldstein J, Tosato G (1999) *Blood* 93:1612–1621.
26. Bix M, Liao NS, Zijlstra M, Loring J, Jaenisch R, Raulet D (1991) *Nature* 349:329–331.
27. Seli E, Arici A (2003) *Semin Reprod Med* 21:135–144.
28. Bussolati B, Deambrosis I, Russo S, Deregibus MC, Camussi G (2003) *FASEB J* 17:1159–1161.
29. Gazvani R, Templeton A (2002) *Reproduction* 123:217–226.
30. Dabrosin C, Gyorffy S, Margetts P, Ross C, Gauldie J (2002) *Am J Pathol* 161:909–918.
31. Maruyama T, Yoshimura Y, Yodoi J, Sabe H (1999) *Endocrinology* 140:2632–2636.
32. Sakai N, Maruyama T, Sakurai R, Masuda H, Yamamoto Y, Shimizu A, Kishi I, Asada H, Yamagoe S, Yoshimura Y (2003) *J Biol Chem* 278:16675–16682.
33. Miyoshi H, Blomer U, Takahashi M, Gage FH, Verma IM (1998) *J Virol* 72:8150–8157.

JOURNAL OF VIROLOGY, Jan. 2007, p. 677–688 Vol. 81, No. 2
0022-538X/07/$08.00+0 doi:10.1128/JVI.00870-06

Nuclear Import of the Preintegration Complex Is Blocked upon Infection by Human Immunodeficiency Virus Type 1 in Mouse Cells[▽]

Naomi Tsurutani,[1]† Jiro Yasuda,[1,2] Naoki Yamamoto,[3] Byung-Il Choi,[1] Motohiko Kadoki,[1] and Yoichiro Iwakura[1]*

Center for Experimental Medicine, Institute of Medical Science, University of Tokyo, Tokyo 108-8639,[1] Fifth Biology Section for Microbiology, Department of First Forensic Science, National Research Institute of Police Science, Kashiwa 277-0882,[2] and Department of Molecular Virology, School of Medicine, Tokyo Medical and Dental University, Tokyo 113-8510,[3] Japan

Received 28 April 2006/Accepted 17 October 2006

Mouse cells do not support human immunodeficiency virus type 1 (HIV-1) replication because of host range barriers at steps including virus entry, transcription, RNA splicing, polyprotein processing, assembly, and release. The exact mechanisms for the suppression, however, are not completely understood. To elucidate further the barriers against HIV-1 replication in mouse cells, we analyzed the replication of the virus in lymphocytes from human CD4/CXCR4 transgenic mice. Although primary splenocytes and thymocytes allowed the entry and reverse transcription of HIV-1, the integration efficiency of the viral DNA was greatly reduced in these cells relative to human peripheral blood mononuclear cells, suggesting an additional block(s) before or at the point of host chromosome integration of the viral DNA. Preintegration processes were further analyzed using HIV-1 pseudotyped viruses. The reverse transcription step of HIV-1 pseudotyped with the envelope of murine leukemia virus or vesicular stomatitis virus glycoprotein was efficiently supported in both human and mouse cells, but nuclear import of the preintegration complex (PIC) of HIV-1 was blocked in mouse cells. We found that green fluorescent protein (GFP)-labeled HIV-1 integrase, which is known to be important in the nuclear localization of the PIC, could not be imported into the nucleus of mouse cells, in contrast to human cells. On the other hand, GFP-Vpr localized exclusively to the nuclei of both mouse and human cells. These observations suggest that, due to the dysfunction of integrase, the nuclear localization of PIC is suppressed in mouse cells.

A small animal model for AIDS would provide a valuable tool for the study of its pathogenesis and the evaluation of vaccine candidates and antiviral drugs. However, attempts to produce small animal models have been hampered thus far by species-specific host range barriers to infection by human immunodeficiency virus type 1 (HIV-1). CD4, the cellular receptor for HIV-1 (41, 49), was first identified as a host range barrier because mouse CD4 (muCD4) does not bind HIV-1 Env (46). Human CD4 (huCD4) transgenic (Tg) mice, however, were not susceptible to HIV-1 infection, suggesting the presence of additional barriers (47). Chemokine receptors were later identified as entry coreceptors (9, 22), but primary lymphocytes from mice transgenic for huCD4 and either huCXCR4 (70) or huCCR5 (13) exhibited little to no signs of productive infection.

Cyclin T1 (CycT1) is responsible for a transcriptional level barrier (3, 4, 26, 30, 58). CycT1 protein is a component of the TAK/pTEFb transcription factor complex (51, 78), and huCycT1 binds Tat and activates transcription from the promoter in the long terminal repeat (LTR). However, muCycT1 cannot bind Tat. Nevertheless, introduction of the huCycT1 protein to rodent cells together with a mixture of human receptors was insufficient to induce productive viral infection (11, 52).

Additional barriers have been reported in the late steps of the viral life cycle (11, 27, 40, 42, 43, 53). These late-stage defects can be rescued by fusing HIV-1-infected rodent cells to uninfected human cells (11, 52), indicating that the defects are due to the lack of necessary factors in rodent cells rather than the presence of dominant inhibitors of HIV-1 replication. CRM1, a nuclear export factor that functions in association with Rev, and p32, a splicing inhibitor and Rev-binding protein, are suggested to be necessary late-phase factors (67, 83).

We previously produced Tg mice carrying the HIV-1 proviral genome in which the *pol* gene is deleted (HIV-Tg) (36). Although transgene expression in lymphoid tissues is barely detectable under normal physiological conditions, relatively high levels of p24 Gag protein were detected in the serum (up to 400 pg/ml) after injection of bacterial lipopolysaccharide (74). All mRNA species, including unspliced, singly spliced, and multiply spliced mRNAs were produced normally. Thus, once the viral genome is integrated into the host chromosome, viral genes are expressed at a reasonable efficiency even in mouse cells, suggesting that the major host range barriers are present in the early stage of infection (prior to viral DNA integration) rather than in the late stage. However, it is not yet known whether there are any additional host range barriers in the early steps.

* Corresponding author. Mailing address: Center for Experimental Medicine, Institute of Medical Science, University of Tokyo, 4-6-1 Shirokanedai, Minato-ku, Tokyo 108-8639, Japan. Phone: 81 3 5449 5536. Fax: 81 3 5449 5430. E-mail: iwakura@ims.u-tokyo.ac.jp.

† Present address: Laboratory of Viral Infection II, Kitasato Institute for Life Sciences, Kitasato University, Tokyo 108-8641, Japan.

▽ Published ahead of print on 1 November 2006.

In this report, we investigated additional barrier steps of HIV-1 replication in mouse cells and found that the efficiency of viral genome integration into the host chromosome was low in huCD4/CXCR4 Tg mice. As this result suggested an additional barrier in the early steps of viral infection, we examined nuclear transport of the viral genome and demonstrated that integrase (IN)-dependent nuclear import of the preintegration complex (PIC) is blocked in mouse cells.

MATERIALS AND METHODS

Transgene construction. The huCD4 Tg vector (pCT4) was constructed as follows. The 0.85-kb XhoI-EcoRV fragment containing the muCD4 enhancer/promoter was ligated to a 1.8-kb EcoRV-HindIII fragment containing the huCD4 open reading frame, and then a 1.95-kb HindIII-SpeI fragment containing a rabbit β-globin intron sequence and a simian virus 40 (SV40) polyadenylation [poly(A)] signal was inserted into the HindIII-SpeI site downstream of the huCD4 gene (29) (Fig. 1A). To construct the huCXCR4 Tg vector, an XhoI-NotI fragment containing the entire coding region of huCXCR4 was isolated from pBCMGSNeo/HM89 (61), and the huCXCR4 fragment was blunted by T4 DNA polymerase, followed by insertion into the EcoRV site of pCDGH. pCDGH consisted of the muCD4 enhancer/promoter and a human growth hormone gene with its poly(A) signal but devoid of its initiation codon (pCFG) (80) (Fig. 1A). The XhoI-SpeI fragment from pCT4 and the XhoI-NotI fragment from pCFG were then purified and coinjected into the male pronuclei of fertilized mouse eggs (C3H/HeN) (80). The transgenes were detected by dot blot hybridization using DNA prepared from mouse tails (34). Mice were kept under specific-pathogen-free conditions in an environmentally controlled clean room at the Center for Experimental Medicine, the Institute of Medical Science, the University of Tokyo. All equipment and supplies were sterilized, including the cages, water bottles, wood chips, and food pellets. All experiments were conducted according to the institutional ethical and safety guidelines for animal experiments and safety guidelines for gene manipulation experiments.

Northern blot hybridization. Northern blot analyses were carried out as previously described (80). The EcoRV-SpeI fragment of huCD4 and the XhoI-NotI fragment of huCXCR4 used for transgene construction were used as templates to make probes detecting huCD4 and huCXCR4 mRNA, respectively. The autoradiograms were developed, and the radioactivity of each band was quantified with a BAS 2000 Bio-Image analyzer (Fuji Film, Tokyo, Japan).

Plasmids. The HIV-1 pNL4-3 (X4-tropic, accession no. M19921) vector was obtained from A. Adachi (1). The HIV-1 pNL43lucΔenv vector, in which the *env* gene is defective and the *nef* gene is replaced by the firefly luciferase (*Luc*) gene, the pNL4-3 vector containing a mutation at the IN catalytic site (D116G), and an amphotropic Moloney murine leukemia virus (MuLV) envelope expression vector (pJD-1) were kindly provided by T. Masuda (54, 65, 76). A vesicular stomatitis virus G (VSV-G)-expressing plasmid (pMD-G) was obtained from L. Naldini (5, 62). The pGEM/NL-2-LTR plasmid was kindly provided by Y. Koyanagi (73).

The HIV-1 pNL43lucΔenv vector carrying a IN protein tagged with the SV40 nuclear localization signal (NLS) was constructed by using overlap extension PCR (33). First, two different PCRs were performed using HIV-1 pNL43lucΔenv vector as the template: one with the AflII-sense primer, 5′-CATCTTAAGACA GCAGTACAAATGGCAGTA-3′, and NLS-antisense primer, 5′-GGCCTTTC TCTTCTTTTTTGGATCCTCATCCTGTCTACTTGCC-3′, and the other with the NLS-sense primer, 5′-CCAAAAAAGAAGAGAAAGGCCTAACACATG GAAAAGATTAGT-3′, and PflMI-antisense primer, 5′-CTCTTTTTCCTCCA TTCTATGGAGACTCCCTG-3′. These two PCR amplicons were then combined and used as the template for the third PCR with outer primers AflII-sense and PflMI-antisense. The final PCR product was digested with AflII and PflMI and ligated to the SpeI/AflII and SpeI/PflMI vector fragments of HIV-1 pNL43lucΔenv. The nucleotide sequence of the construct was confirmed by sequencing.

To prepare the expression vector for HIV-1 IN N-terminal fusion to enhanced green fluorescence protein (EGFP) (GFP-IN), the entire coding region of HIV-1 IN was amplified by PCR and inserted into the pEGFP-C2 expression vector (Clontech Laboratories, Palo Alto, CA) at its EcoRI and ApaI sites. The primers used to amplify the HIV IN were GFP-IN-sense, 5′-CCGGAATTCCGGGCC ATAGCGGCCTTTTTAGATGGAATAGAT-3′, and GFP-IN-antisense, 5′-TC CGGGCCCGGATTAATCCTCATCCTGTCTACT-3′. To generate the expression vector for the HIV-1 Vpr N or C terminus fused to EGFP (GFP-Vpr, Vpr-GFP), the entire coding region of HIV-1 Vpr was amplified by PCR and inserted into the pEGFP-C2 or pEGFP-N1 expression vector at the HindIII and ApaI or HindIII and BamHI sites, respectively. The primers used to amplify HIV-1 Vpr were GFP-Vpr-sense, 5′-CCCAAGCTTGGGGGACGCCATGGA ACAAGCCCCAGAA-3′, and GFP-Vpr-antisense, 5′-TCCGGGCCCGGACT AGGATCTACTGGCTCCATT-3′, or Vpr-GFP-sense, 5′-CCCAAGCTTGGG GACATGGAACAAGCCCCAGAA-3′, and Vpr-GFP-antisense, 5′-CGCGGA TCCGCGGAGGATCTACTGGCTCCATT-3′, respectively. The amplified regions and the cloning junctions were confirmed by DNA sequencing.

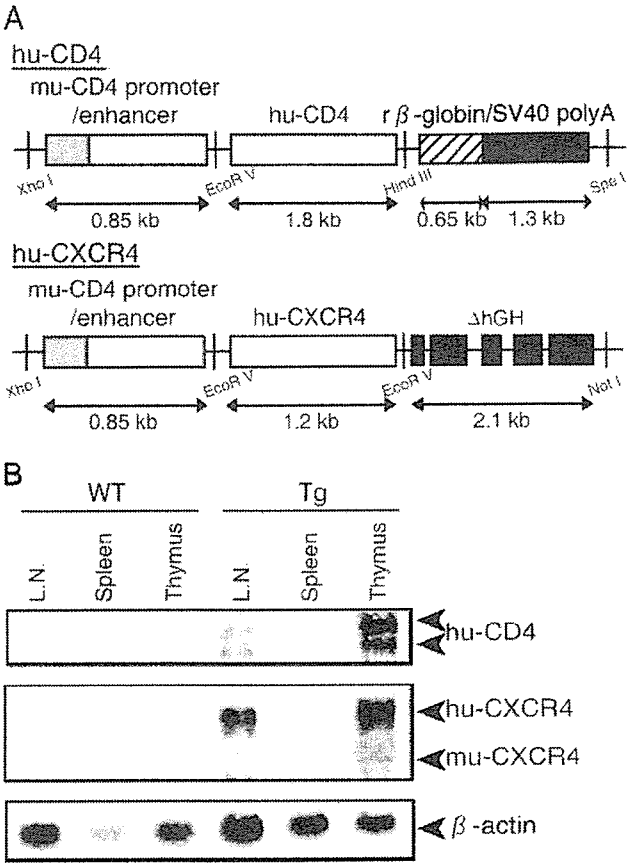

FIG. 1. (A) Transgene constructs. huCD4 or CXCR4 cDNA was placed downstream of the muCD4 enhancer/promoter and ligated to the SV40 poly(A) signal (huCD4) or to a defective human growth hormone gene containing the poly(A) signal (huCXCR4). (B) Transgene expression in lymphatic organs. Northern blot hybridization analysis was performed using 10 μg of total RNA prepared from the thymus, spleen, or lymph nodes of WT or Tg mice. The positions expected for huCD4, huCXCR4, muCXCR4, and β-actin mRNA are indicated on the right.

Cell culture and isolation of human PBMCs and mouse splenocytes and thymocytes. Human fibroblast-like cell lines (293T and HeLa), a mouse embryo fibroblast-like cell line (NIH 3T3) derived from an NIH Swiss mouse (Fv-1^n), and a mouse rectum carcinoma cell line (Colon-26) from a BALB/c mouse (Fv-1^b) were cultured in Dulbecco's modified Eagle's medium (Invitrogen, Tokyo, Japan) supplemented with 10% fetal bovine serum (FBS). The Colon-26 cell line was obtained provided from the Cell Resource Center for Biomedical Research Institute of Development, Aging, and Cancer, Tohoku University, Japan (75). Human T-cell lymphoma cell lines (MT-4 and Jurkat) and mouse T-cell lymphoma cell lines (EL4, YAC-1, and BW5147) were cultured in RPMI 1640 (SIGMA, Tokyo, Japan) containing 10% FBS. Human peripheral blood mononuclear cells (PBMCs) were obtained from peripheral blood. Briefly, buffy coats from the peripheral blood of healthy HIV-seronegative blood donors were separated over a Ficoll-Hypaque gradient (Ficoll-Paque PLUS; GE Healthcare Bio-Sciences, Tokyo, Japan). C3H/HeN mice (Charles River, Tokyo, Japan) were sacrificed at 8 weeks, and the splenocytes and thymocytes were isolated by passage through nylon mesh. Human PBMC suspensions and mouse splenocytes

and thymocytes were stimulated with 1% phytohemagglutinin (SIGMA, Tokyo, Japan). These cells were grown in RPMI 1640 medium containing 4 ng/ml of recombinant human interleukin 2 or mouse interleukin 2 (Peprotech EC Ltd, London, United Kingdom) per ml and 10% FBS. After 1 week, human PBMCs and mouse splenocytes and thymocytes were >96% T cells and >40% activated cells, as judged by fluorescence-activated cell sorter analysis using anti-CD3 or anti-CD69 monoclonal antibodies (BD Biosciences, Tokyo, Japan), respectively (data not shown).

Virus preparation and infection assays. HIV-1 strain NL4-3 was propagated in MT-4 cells, and the supernatants were filtered and stored at −80°C until use. For single-round infection assays, pseudotyped viruses were generated by cotransfection of 293T cells with pNL43lucΔenv vector and an amphotropic Moloney MuLV envelope expression vector (pJD-1) or a VSV-G envelope expression vector (pMD-G) using Lipofectamine PLUS (Invitrogen) (76). The pNL43lucΔenv vector containing a mutation at the IN catalytic site (D116G) was used as a control (54). The culture supernatants of the transfected 293T cells were harvested at 48 h posttransfection, filtered through 0.45-μm filters, and used as the virus preparations. Each virus preparation was treated with DNase I (40 μg/ml; Worthington Biochemical Co., Lakewood, NJ) in the presence of 10 mM $MgCl_2$ at 37°C for 1 h to avoid DNA contamination. An aliquot of each virus preparation was incubated at 65°C for 1 h and used as a heat-inactivated control. To monitor viral gene expression from the pNL43lucΔenv vector carrying a IN protein tagged with the SV40 NLS, luciferase activity in transfected 293T cells was measured on a Lumat LB9507 luminometer (BERTHOLD, Technologies, Bad Wildbad, Germany). At 48 h posttransfection, 293T cells were lysed with 1 ml of luciferase lysis buffer (Promega). One microliter of each cell lysate was subjected to the luciferase assay. Human PBMCs (5×10^6) or HeLa (5×10^5), MT-4 (5×10^6), Jurkat (5×10^6), mouse splenocytes (5×10^6), mouse thymocytes (5×10^6), NIH 3T3 (5×10^5), BW5147 (5×10^6), EL4 (5×10^6), or YAC-1 (5×10^6) cells were infected with an aliquot (2 ml; containing approximately 500 ng [NL4-3], 200 ng [HIV-1/MuLV], or 50 ng [HIV-1/VSV-G] of p24) of DNase-treated virus. The infection proceeded in the presence of Polybrene (SIGMA, Tokyo, Japan) (10 μg/ml) at 37°C. After 6 h, the viruses were removed, and the cells were overlaid with fresh media and incubated at 37°C. For p24 CA analysis, the infected cell supernatants were removed on the indicated days following infection. The levels of HIV-1 p24 antigen were determined by an enzyme immunoassay system (RETRO-TEK; ZeptoMetrix Corp., Buffalo, NY). For luciferase analysis, infected cells were harvested 4 days after infection, and the total cell pellets from each well were washed twice with phosphate-buffered saline (PBS) and lysed in luciferase lysis buffer (Promega). Luciferase activity (measured in a relative light units [RLU]) was measured on a Lumat LB9507 luminometer (BERTHOLD, Technologies, Bad Wildbad, Germany).

Analysis of HIV-1 DNA synthesis and formation of 2-LTR circles. Cells were harvested 24 h after infection. After washing with PBS, nucleic acids were extracted as described previously (81). Briefly, cells were disrupted in urea lysis buffer (4.7 M urea, 1.3%, sodium dodecyl sulfate [SDS], 0.23 M NaCl, 0.67 mM EDTA, and 6.7 mM Tris-HCl [pH 8.0]), phenol-chloroform extracted, and ethanol precipitated. The DNA pellet was resuspended in distilled H_2O, and an aliquot of each sample was analyzed by PCR. For ex vivo infection of primary lymphocytes from huCD4/CXCR4 Tg mice, partial reverse transcripts of the viral DNA were quantified by semiquantitative PCR. The primers used were as follows (37, 45, 81): R-U5, R, 5′-GCCTCAATAAAGCTTGCCTTG-3′ (sense, positions 522 to 542); U5, 5′-CCACTGCTAGAGATTTTCCAC-3′ (antisense, positions 616 to 638); Gag forward, 5′-TGGGGGGACATCAAGCAGCCATG CA-3′ (sense, positions 1360 to 1385); Gag reverse, 5′-CTATGTCACTTCCCC TTGGTTCTCT-3′ (antisense, positions 1474 to 1498). The PCR program was 30 cycles at 95°C for 1 min, 60°C for 1 min, and 72°C for 1 min in the presence of [^{32}P]dCTP. The PCR products were electrophoresed on an 8% polyacrylamide–Tris-borate-EDTA gel. The autoradiograms were developed, and the radioactivity of each band was quantified by a BAS 2000 Bio-Image analyzer. For single-round infections, the DNA was measured by quantitative PCR using an ABI PRISM 7900HT qPCR machine (Applied Biosystems, Tokyo, Japan). The PCR primer pairs were as follows: R-U5 (M667/AA55), R-gag (M667/M661) (76), and the 2-LTR junction's sequence (2-LTR-S/2-LTR-AS) (73). The cycling conditions included a hot start (50°C for 2 min, 95°C for 10 min), followed by 40 cycles of denaturation (95°C for 15 s) and extension (60°C for 1 min). To compensate for varying DNA sample recovery, the data are presented as ratios of HIV-1 DNA to β-actin DNA.

Cassette ligation-mediated PCR and integration analysis. For the detection of the HIV-1 integration form, we designed a cassette ligation-mediated PCR system using an in vitro LA cloning kit (TaKaRa BIO, Shiga, Japan) (35) (see Fig. 3A). Briefly, 5 μg of DNA was digested with EcoRI and ligated to double-stranded DNA cassettes with compatible ends. The cassette-ligated restriction fragments were then subjected to two rounds of PCR using the cassette- and HIV-specific primers C1 (5′-GTACATATTGTCGTTAGAACGCGTAATACG ACTCA-3′) and Gag reverse (described above) for the cassette, *gag*, and its upstream region and C2 (5′-CGTTAGAACGCGTAATACGACTCACTATAG GGAGA-3′) and U5 reverse (described above) for the cassette sequence downstream of C1 and the LTR region. PCR was performed according to the manufacturer's instructions. The amplification conditions were 30 cycles of 1 min at 94°C, 2 min at 54°C, 2 min at 72°C, and a final extension of 1 min at 72°C. The amplified products were resolved on 2% agarose gels and stained with SYBR green (FMC Bioproduct, Rockland, ME).

Fluorescence microscopy. HeLa (4×10^4), NIH 3T3 (3×10^4), and Colon-26 (3×10^4) cells were seeded onto 8-well culture slides (Nalge Nunc International, Rochester, NY) and transfected with the indicated plasmids using Lipofectamine 2000 (Invitrogen). At 24 h posttransfection, the cells were washed once in PBS and fixed with acetone for 5 min. After washing with PBS, the cells were mounted in 90% glycerol–50 mM $NaHCO_3$-Na_2CO_3 and covered by a coverslip. Confocal microscopy was performed with a Nikon Optiphot-2 fluorescence microscope with a Bio-Rad MRC 1024 laser confocal imaging system, and the digital images were prepared using Adobe Photoshop software.

Particle preparation and Western blot analysis. The culture supernatant (5 ml) of HIV-1 producing plasmid-transfected 293T cells was collected at 48 h postinfection. It was centrifuged thorough 20% (wt/vol) sucrose–PBS in an SW55 rotor (Beckman Coulter) at 4°C at 147,000 × *g* for 2 h (56), and the pellet was resuspended in PBS. The viral pellets were heated at 90°C for 10 min in the presence of sample buffer (62.5 mM Tris-HCl, pH 6.8, 10% glycerol, 2% SDS, 5% 2-mercaptoethanol, 0.005% bromophenol blue). Then viral proteins were electrophoresed on a 12% SDS–polyacrylamide gel containing 0.2% SDS. Following blotting of proteins onto a polyvinylidene difluoride membrane, the membrane was first incubated with an antiserum from an AIDS patient (provided by Y. Inagaki, Tokyo Medical and Dental University, Tokyo, Japan, and Y. Koyanagi, Kyoto University, Kyoto, Japan), followed by horseradish peroxidase-conjugated anti-human immunoglobulin. HIV-1 proteins were visualized using an enhanced chemiluminescence detection system (GE Healthcare Bio-Science, Tokyo, Japan).

Statistical analysis. Data were analyzed using Excel and Student's *t* test. A *P* value of <0.05 was considered statistically significant, and all results are presented as means ± standard errors of the means (SEM).

RESULTS

Lymphocytes from huCD4/CXCR4 Tg mice do not fully support HIV-1 infection. To elucidate the host range barriers of HIV-1 replication in mice, we analyzed the early processes of HIV-1 infection in huCD4/CXCR4 Tg mouse splenocytes. Transgenic mice were generated by introducing both huCD4 and huCXCR4 cDNA along with the muCD4 enhancer/promoter into fertilized C3H mouse eggs (Fig. 1A). As shown in Fig. 1B, the huCD4 and huCXCR4 mRNAs were detected mostly in the thymus but also in the lymph nodes and spleen. Two huCD4 mRNA species were detected due to alternative splicing of the SV40 gene that was ligated to the huCD4 gene (Fig. 1B). fluorescence-activated cell sorter analyses showed that Tg splenocytes and thymocytes both expressed huCD4 and huCXCR4 on their cell surfaces (data not shown).

To examine the susceptibility of these Tg mice to HIV infection, splenocytes and thymocytes were isolated from the mice and infected with T-tropic HIV-1 (NL4-3) or M-tropic HIV-1 (JR-CSF). However, we could not detect any p24 antigen in the culture supernatant of these Tg mouse-derived cells, although significant levels of p24 (up to 80 pg/ml) were produced in human PBMC culture supernatant 12 days after infection.

To determine the process by which the viral replication is blocked, we analyzed the early infection steps by examining the viral genomic structure. Twenty-four hours after HIV-1 infection of the huCD4/CXCR4 Tg splenocytes, cells were har-

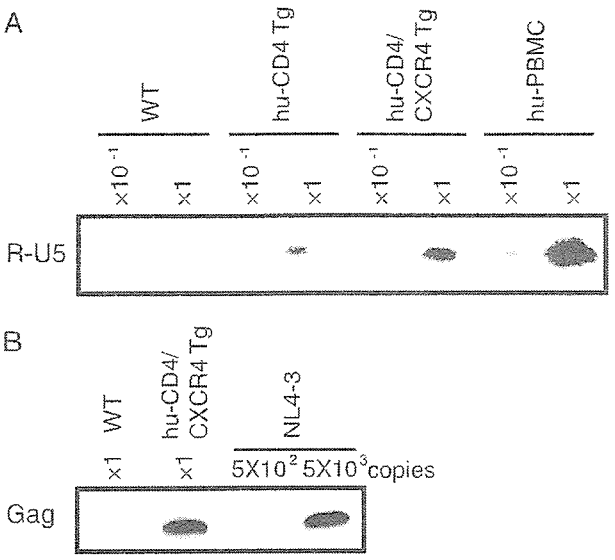

FIG. 2. HIV infection of splenocytes and thymocytes of WT and huCD4/CXCR4 Tg mice. Splenocytes or thymocytes from WT mice, Tg mice, or human PBMCs were isolated and infected with equivalent amounts of DNase-treated NL4-3 virus at 37°C for 6 h. After 6 h, the viruses were removed and the cells were treated with trypsin (500 μg/ml) at 37°C for 10 min and then washed in growth medium. (A and B) Splenocytes were harvested at 24 h postinfection. Total DNA was extracted from the cells and subjected to PCR analysis with a primer pair for R/U5 (A) or R/gag (B). The reaction was carried out using the DNA preparation from 1×10^5 cells (×1) or 1×10^4 cells ($\times 10^{-1}$). In panel B, the lanes marked 5×10^2 and 5×10^3 represent PCR products using 5×10^2 or 5×10^3 copies of the pNL4-3 plasmid as the template.

vested and total DNA was extracted. Early (R-U5) and late-infectious intermediate products (R-gag) were determined using semiquantitative PCR with specific primers. As shown in Fig. 2A and B, both infectious intermediates were detected specifically in the DNA isolated from the splenocytes of huCD4/CXCR4 Tg mice exposed to HIV-1, indicating that viral entry and reverse transcription had proceeded normally in mouse cells provided that human viral receptors were supplied. Similar results were also obtained in huCD4/CCR5 Tg mouse splenocytes infected with HIV-1 JR-CSF (data not shown). In contrast, the early infectious intermediate was not detected in wild-type mouse splenocytes, indicating a block upon viral entry. Taken together, these results suggest that HIV-1 replication in huCD4/CXCR4 Tg splenocytes was blocked later than the reverse transcription step(s).

HIV-1 infection of mouse cells is blocked at steps preceding integration into the host chromosome. We next examined the integration of the HIV-1 genome into the host chromosome. The pNL4-3 vector containing a mutation at the IN catalytic site (D116G) was used as a control (54). DNA from the infected cells was digested with EcoRI, which cut proviral DNA at only one site (nucleotide number 5743 of NL4-3, accession no. M19921). The DNA was then ligated to an EcoRI-specific cassette and subjected to the first round of PCR using primers specific for the cassette and the *gag* region, followed by the second round of PCR using primers for the cassette and the LTR region (Fig. 3A). As a result, the integrated viral DNA was visualized as smearing bands greater than 638 bp, which is

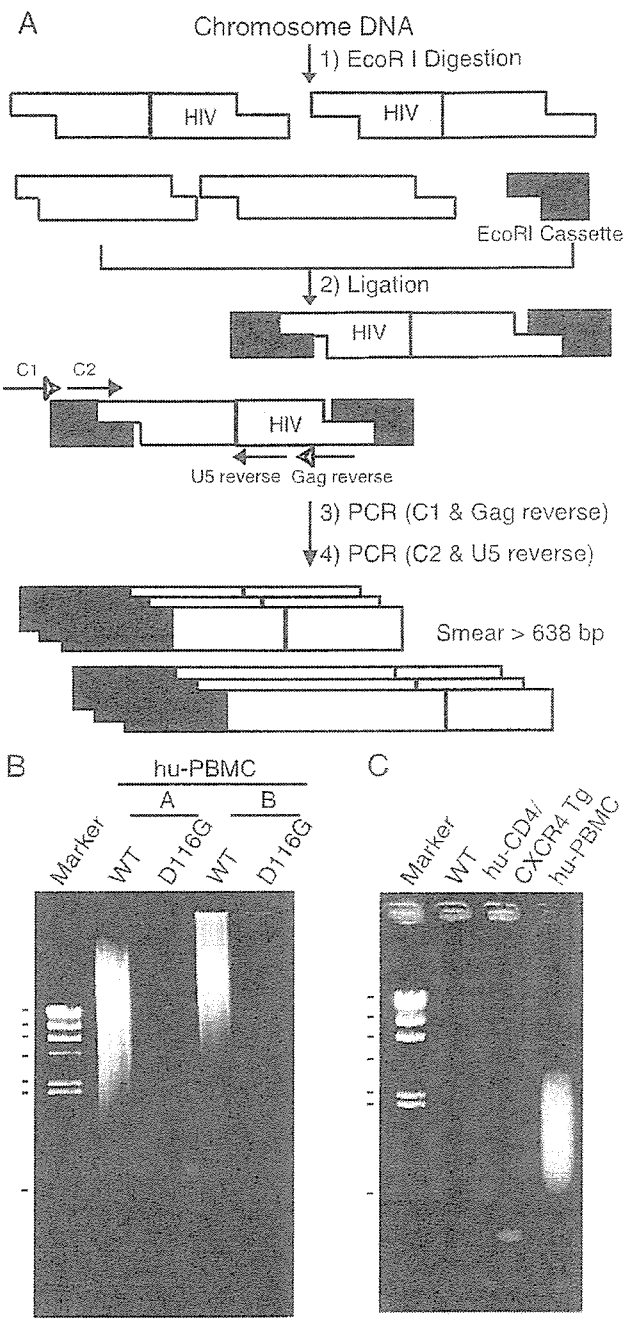

FIG. 3. Suppression of NL4-3 virus DNA integration in the mouse chromosome. Human PBMCs and murine splenocytes were infected with equivalent doses of DNase-treated NL4-3 virus. After 6 h, the virus was removed and the cells were washed with growth medium. At 1 day postinfection, the cells were harvested and used to extract total DNA. The DNA (5 μg) was digested with EcoRI and ligated to double-stranded DNA cassettes with compatible ends. The cassette-ligated DNA fragments were used as templates for nested PCR using cassette- and HIV-specific primers. (A) Schematic representation of cassette ligation-mediated PCR and the primers used to detect HIV integration into the host chromosome. (B and C) Detection of the chromosome-integrated forms of viral DNA. (B) Human PBMC preparations from two donors (A and B) were infected with NL4-3-WT or integrase mutant (D116G), and the DNAs were subjected to PCR analysis. Markers: 23.1, 9.4, 6.6, 4.3, 2.3, 2.0, and 0.564 kb (λ/HindIII). (C) DNA was isolated from NL4-3-infected splenocytes or thymocytes from WT or Tg mice or human PBMCs following infection and subjected to PCR analysis. Note the smearing bands in virus-infected human PBMCs but not in huCD4/CXCR4 Tg mice. Marker: λ/HindIII.

the original length between C2 and U5 reverse primers without insertion. Smearing bands were clearly detected when the DNA from HIV-1 wild type (WT)-infected human PBMCs was analyzed. In contrast, no smearing bands were detected with the DNA from HIV-1-D116G infected human PBMC, HIV-1-WT infected splenocytes from WT, and huCD4/CXCR4 transgenic mice (Fig. 3B and C). These results suggest that HIV-1 replication is also blocked in mouse cells at steps between the entry and viral DNA integration steps or at the viral integration step in addition to the adhesion/entry step.

The infection of mouse cells with both HIV-1/pJD-1 and HIV-1/VSV-G pseudotyped virus are blocked at a postentry step. To examine the possibility that HIV-1 replication in mouse cells is blocked at steps between the viral entry and DNA integration steps, we analyzed the early steps of viral infection using HIV-1 pseudotyped viruses in which the Env is replaced by an amphotropic MuLV Env (HIV-1/pJD-1) or by the G protein of VSV (HIV-1/VSV-G) and the *nef* gene is replaced by the firefly luciferase gene (76). The MuLV envelope pseudotype uses a ubiquitously expressed phosphate transporter as the receptor (55), and the VSV-G envelope pseudotype is capable of infecting cells through a carbohydrate receptor and the endocytic pathway (2). By using these pseudotyped viruses, we overcame the barriers at the adhesion and entry steps.

Among the adherent cells tested, 293T and HeLa cells showed high luciferase activity upon infection with both types of pseudotyped viruses, whereas NIH 3T3 cells yielded 10- to 100-fold-lower signals (Fig. 4). Similarly, the mouse T-cell lines BW5147, EL4, and YAC-1 displayed 100- to 1,000-fold-lower signals than did the human T-cell lines MT4 and Jurkat. Furthermore, luciferase expression efficiency was lower, by more than 1,000-fold, in mouse primary splenocytes than in human PBMCs. The relative sensitivity to infection of these cells was similar between the two pseudotyped viruses, although the efficiency of infection was approximately 10-fold higher in the HIV-1/VSV-G infection. Thus, these results again support a species-specific block in mouse cells subsequent to the entry step.

Reverse transcription of HIV-1 proceeds normally in mouse cells. We next evaluated the ability of mouse cells to support HIV-1 DNA synthesis. One day after infection, total DNA was harvested from various infected cells and subjected to quantitative PCR analyses. Both early (R-U5) and late (R-gag) reverse transcription products were specifically detected in DNA isolated from human and mouse cells exposed to both of the pseudotyped viruses, HIV-1/pJD-1 (Fig. 5A) and HIV-1/VSV-G (Fig. 5B). No R-U5 or R-gag products were detected when heat-inactivated (65°C, 1 h) viruses were infected, indicating that these products were not derived from the transfected HIV-1 DNA carryover. The copy number of R-U5, which reflects the efficiency of viral entry, was higher in mouse cells (NIH 3T3, BW5147, and splenocytes) than in human cells (HeLa, MT4, and PBMCs). The ratio of R-gag/R-U5 was calculated to evaluate the efficiency of the reverse transcription because R-U5 reflects the efficiency of entry (Fig. 5A and B, lower panels). No significant difference in the efficiency of reverse transcription was observed between mouse cells and human cells exposed to HIV-1/pJD-1 (Fig. 5A) and HIV-1/VSV-G (Fig. 5B). These results indicated that mouse cells supported reverse transcription at an efficiency similar to that of human cells.

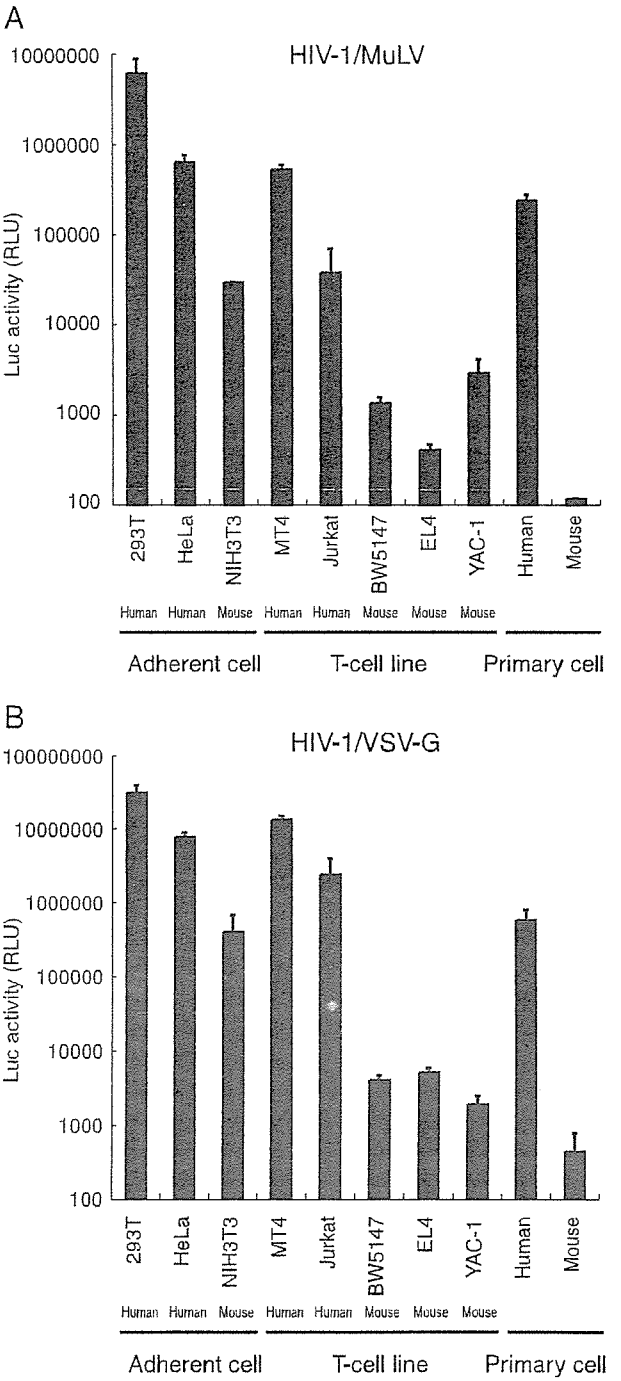

FIG. 4. Analysis of HIV-1 pseudotype virus replication in mouse cells. Human and murine cells were infected with equivalent doses of pNL43lucΔenv that was pseudotyped with either MuLV (A) or VSV-G (B) at 37°C for 6 h. After removal of the virus, cells were washed in growth medium. Luciferase activity was measured at 4 days postinfection, and normalized activities relative to the total protein quantity are shown. The data represent the means ± SEM of results from three wells. The data were reproduced in three independent experiments.

Nuclear import of the PIC is blocked in mouse cells. After completion of reverse transcription, the PIC crosses the

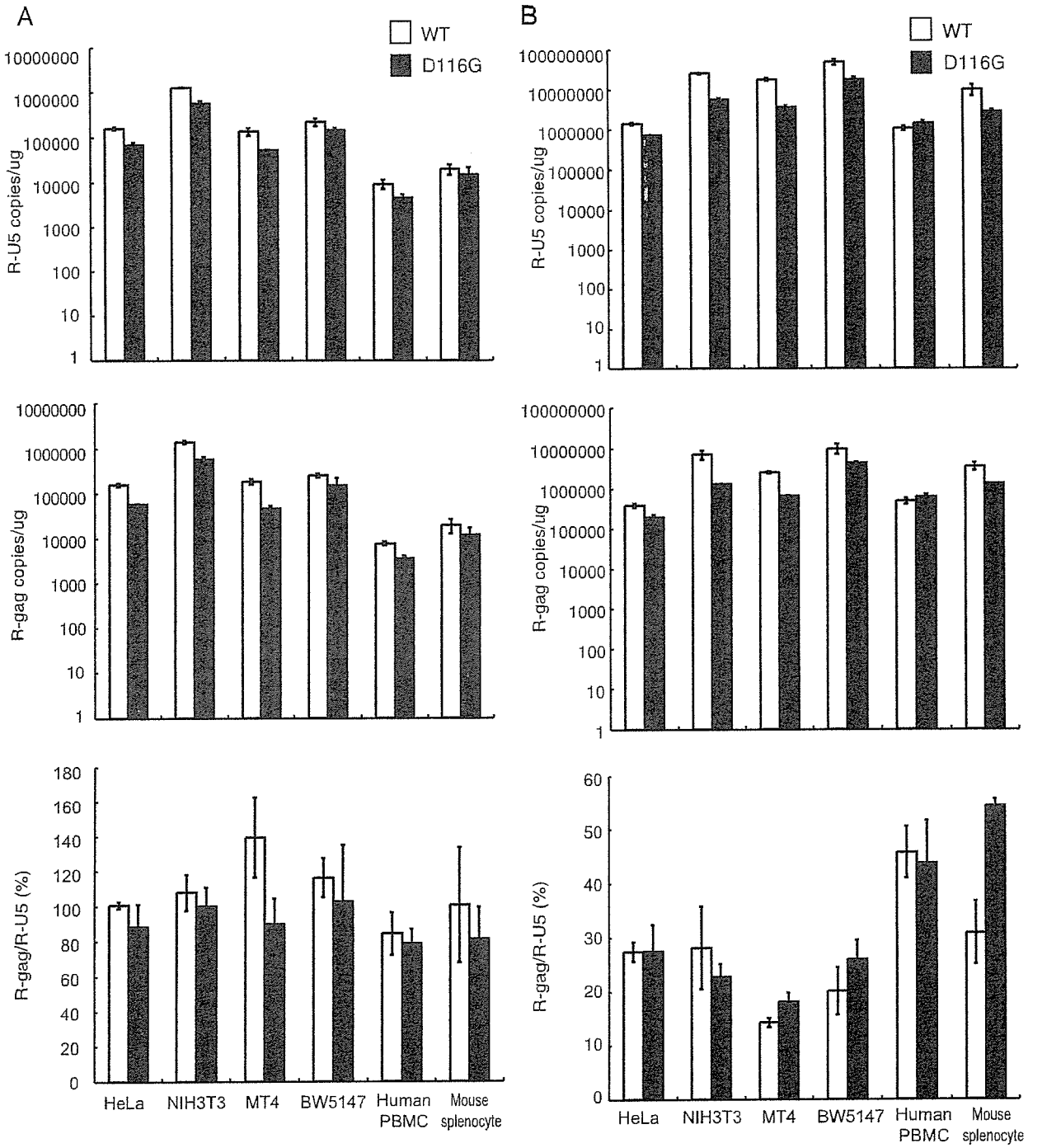

FIG. 5. The efficiency of the reverse transcription of HIV-1 in mouse cells. Human and murine cells were infected with equivalent doses of DNase-treated WT or integrase mutant (D116G) MuLV pseudotyped virus (A) or VSV-G pseudotyped virus (B). At 1 day postinfection, the cells were harvested, and the total DNA was extracted and subjected to quantitative real-time PCR analysis using primer pairs for R/U5 (upper panels) or R/gag (middle panels). The copy numbers of HIV-1 DNA per 1 μg β-actin are shown. The reverse transcription (RT) efficiency is calculated by dividing the late RT product (R-gag) by the early RT product (R-U5) (lower panel). The data represent the means ± SEM of results from three wells. The data were reproduced in three independent experiments.

nuclear membrane and enters the nucleus. Ligases within the nucleus then circularize the proviral DNA (2-LTR containing circular DNA) before its integration into the host chromosome (17, 57, 82). Although these 2-LTR circles are nonfunctional, they can serve as a measure of viral nuclear entry. To assess the efficiency of PIC transport into the nuclei of mouse cells, we estimated de novo-synthesized 2-LTR circular-form DNA by PCR using primer pairs that amplify sequences unique to this DNA form. The fragment corresponding to the 2-LTR circular junction was clearly

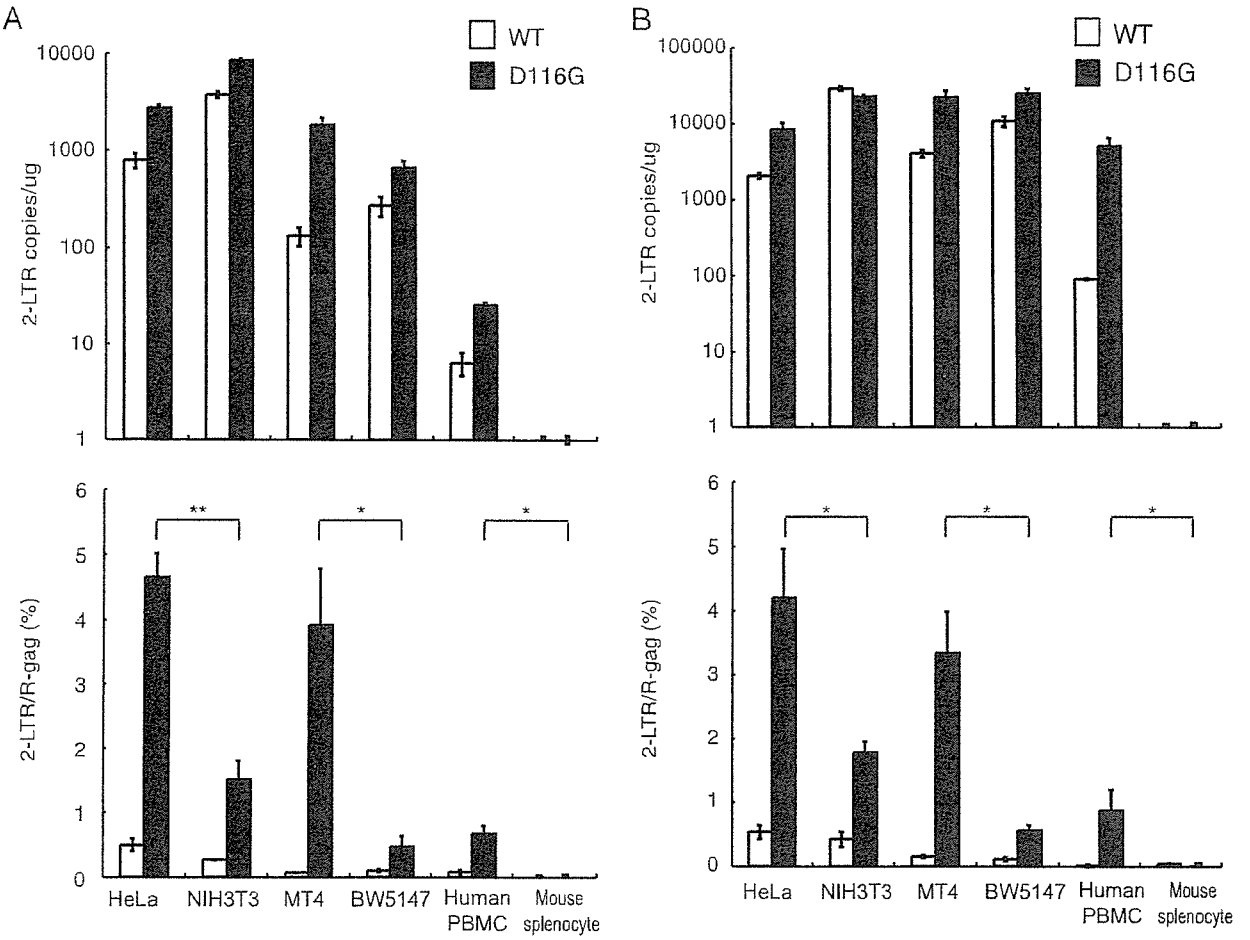

FIG. 6. Suppression of the 2-LTR circular form of DNA in mouse cells. Human and mouse cells were infected with equivalent doses of DNase-treated WT or integrase-mutant (D116G) MuLV pseudotype virus (A) or VSV-G pseudotype virus (B). The DNA from the infected cells was subjected to quantitative real-time PCR analysis using a primer pair specific for the 2-LTR circular form of the DNA (upper panels). The nuclear import efficiency was calculated by dividing the 2-LTR products by the late reverse transcription products (lower panels). The data represent the means ± SEM of results from three wells, and the data were reproduced in three independent experiments. *, $P < 0.05$; **, $P < 0.01$ (determined by Student's t test).

detected at 1 day postinfection in the DNA samples from HeLa, NIH 3T3, MT-4, BW5147, and human PBMCs infected with HIV-1/pJD-1 pseudotyped virus (Fig. 6A, upper panel). However, only a small amount of 2-LTR circle was detected in the mouse splenocytes. A similar tendency was observed in cells infected with the HIV-1/VSV-G pseudotyped virus (Fig. 6B, upper panel). The 2-LTR DNA in mouse cells was also measured at 2 and 4 days postinfection using both pseudotyped viruses and provided similar results (data not shown).

The ratio of 2-LTR/R-gag was calculated to evaluate the efficiency of nuclear import because the copy number of 2-LTR in the nucleus should be dependent on the amount of cytoplasmic R-gag, which represents the precursor of 2-LTR. The efficiency was very low and not significantly different between human and mouse when wild-type HIV-1 pseudovirus was infected (Fig. 6, lower panel). Because the nuclear concentration of 2-LTR is determined by the balance between accumulation of PIC by nuclear import and loss of PIC from the nucleoplasm by chromosome integration, we next used an integration-defective mutant, D116G, to examine only the efficiency of nuclear import. As shown in Fig. 6, the ratio was significantly lower in NIH 3T3 cells than in HeLa cells (33% or 43% of HeLa cells) and in BW5147 cells than in MT4 cells (12% or 17% of MT4 cells) when they were infected with HIV-1/pJD-1 or HIV-1/VSV-G, respectively (Fig. 6A and B, lower panels). We were unable to compare the efficiency of PIC import in human PBMCs and mouse splenocytes because the 2-LTR circle was not detected in mouse splenocytes. These results suggested that the nuclear import of the PIC is blocked in mouse cells, especially in splenocytes.

A block in the nuclear localization of the PIC is caused by a defect in IN nuclear localization. As Vpr and IN play important roles in importing the PIC into the nucleus, we hypothesized that Vpr and/or IN is nonfunctional in mouse cells due to the inability to utilize the cellular factors necessary for trafficking to the nucleus. To directly examine the karyophilic properties of HIV-1 IN in mouse cells, we generated an expression vector with HIV-1 IN in which the N terminus was fused to EGFP (GFP-IN). Since it was reported that β-galactosidase fusion to the C terminus of IN could not be located in

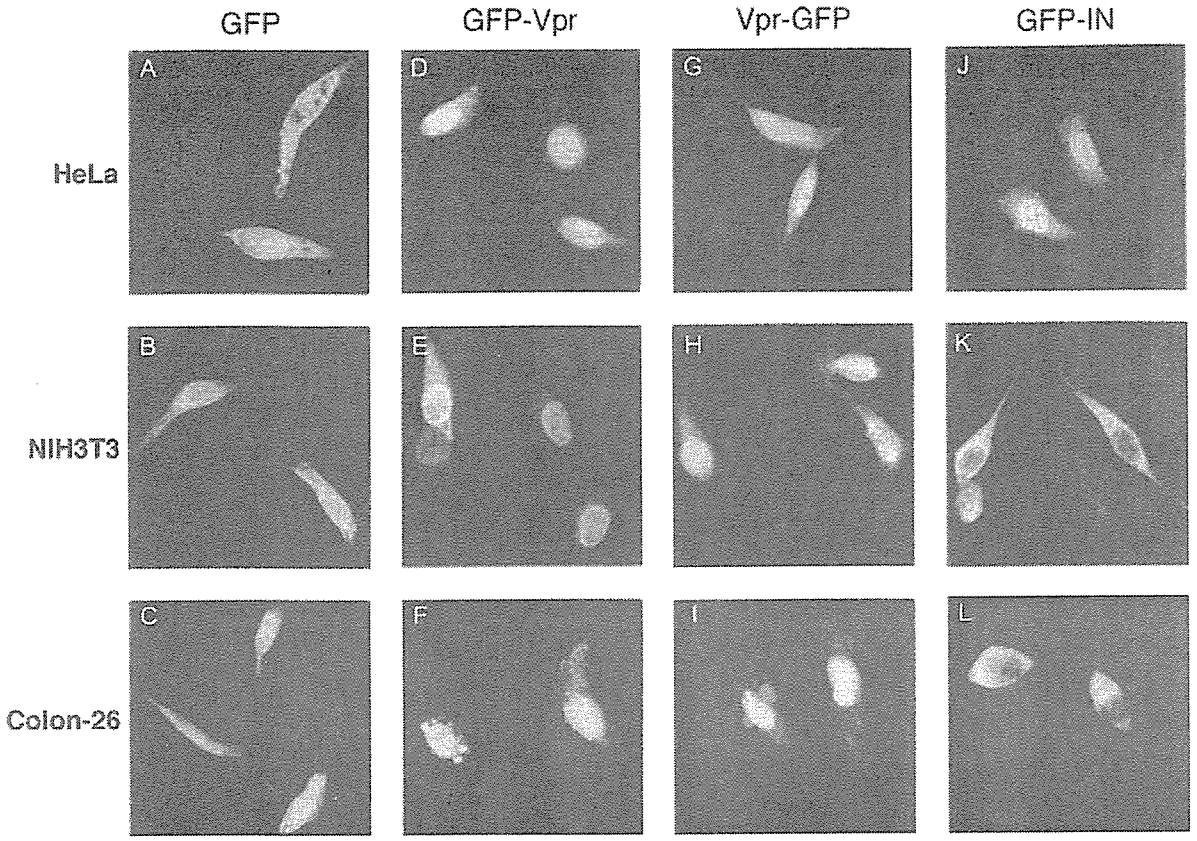

FIG. 7. Inhibition of IN-dependent GFP nuclear import in mouse cells. HeLa (A, D, G, and J), NIH 3T3 (B, E, H, and K), and Colon-26 cells (C, F, I, and L) were transfected with plasmids expressing GFP only (A, B, and C), GFP fused to the HIV-1 Vpr N terminus (GFP-Vpr) (D, E, and F), GFP fused to the HIV-1 Vpr C terminus (Vpr-GFP) (G, H, and I), and GFP fused to HIV-1 IN (J, K, and L) using Lipofectamine 2000. At 24 h posttransfection, the cells were fixed and visualized by confocal fluorescence microscopy. Note that the nuclear localization of GFP-IN is inhibited in mouse cells (K and L).

the nucleus (44), we did not examine the C terminus fusion construct (IN-GFP). We also generated HIV-1 Vpr expression vectors in which the N or C terminus was fused to EGFP (GFP-Vpr and Vpr-GFP, respectively). At 24 h postinfection, HeLa, NIH 3T3, and Colon-26 cells were transfected with the GFP fusion vectors, and the subcellular localization of IN or Vpr was examined with a confocal microscope. We used Colon-26 cells (Fv-1^n) in addition to NIH 3T3 cells (Fv-1^b) because Fv-1 may exert its antiretroviral effect at a postentry step, after reverse transcription and prior to integration (38, 79). Colon-26 cells and NIH 3T3 cells showed similar levels of luciferase activity upon infection with both types of pseudotyped viruses. Control GFP without IN or Vpr was distributed uniformly throughout both the cytoplasm and the nuclei in all cells examined (Fig. 7A to C). GFP-Vpr, on the other hand, accumulated almost exclusively in the nuclei of HeLa (Fig. 7D), NIH 3T3 (Fig. 7E), and Colon-26 (Fig. 7F) cells, although low levels of nuclear membrane association were also observed in NIH 3T3 cells (Fig. 7E). Vpr-GFP also accumulated almost exclusively in the nuclei of HeLa (Fig. 7G), NIH 3T3 (Fig. 7H), and Colon-26 (Fig. 7I) cells. These results indicated that HIV-1 Vpr has strong karyophilic properties and that, even in mouse cells, it can be transported across the nuclear membrane. In contrast, although GFP-IN accumulated almost exclusively in the nuclei of HeLa cells (Fig. 7J), GFP-IN was localized only in the cytoplasm of NIH 3T3 (Fig. 7K) and Colon-26 (Fig. 7L) cells. Thus, our results demonstrate that IN-mediated nuclear transport of HIV-1 PIC is impaired in mouse cells of both Fv-1 genotypes.

Addition of the SV40 NLS to the C terminus of HIV-1 integrase enhances viral infectivity in mouse cells. To analyze the role of IN in nuclear localization of HIV-1, we constructed an HIV-1 pNL43lucΔenv vector with the SV40 NLS at the C terminus of IN (IN-NLS), and pseudotyped virus was generated by cotransfection of 293T cells with the pNL43lucΔenv wild type or IN-NLS vector and VSV-G expression vector. Luciferase activity in the cell lysate of 293T cells transfected with IN-NLS was increased 2.5-fold compared to that transfected with wild-type virus (Fig. 8A). To verify that the gag-pol polyprotein processing was completed in IN-NLS virus particles, we performed Western blot analysis using an AIDS patient serum. No difference of the viral components was observed between parental WT and IN-NLS viruses (Fig. 8B). The content of p24 protein of the IN-NLS was also shown to be normal using a specific monoclonal antibody (data not shown). These results showed that addition of NLS to IN significantly activates viral replication.

Then we tested the susceptibility of HeLa, NIH 3T3, BW5147, and MT4 cells to IN-NLS infection. Addition of the

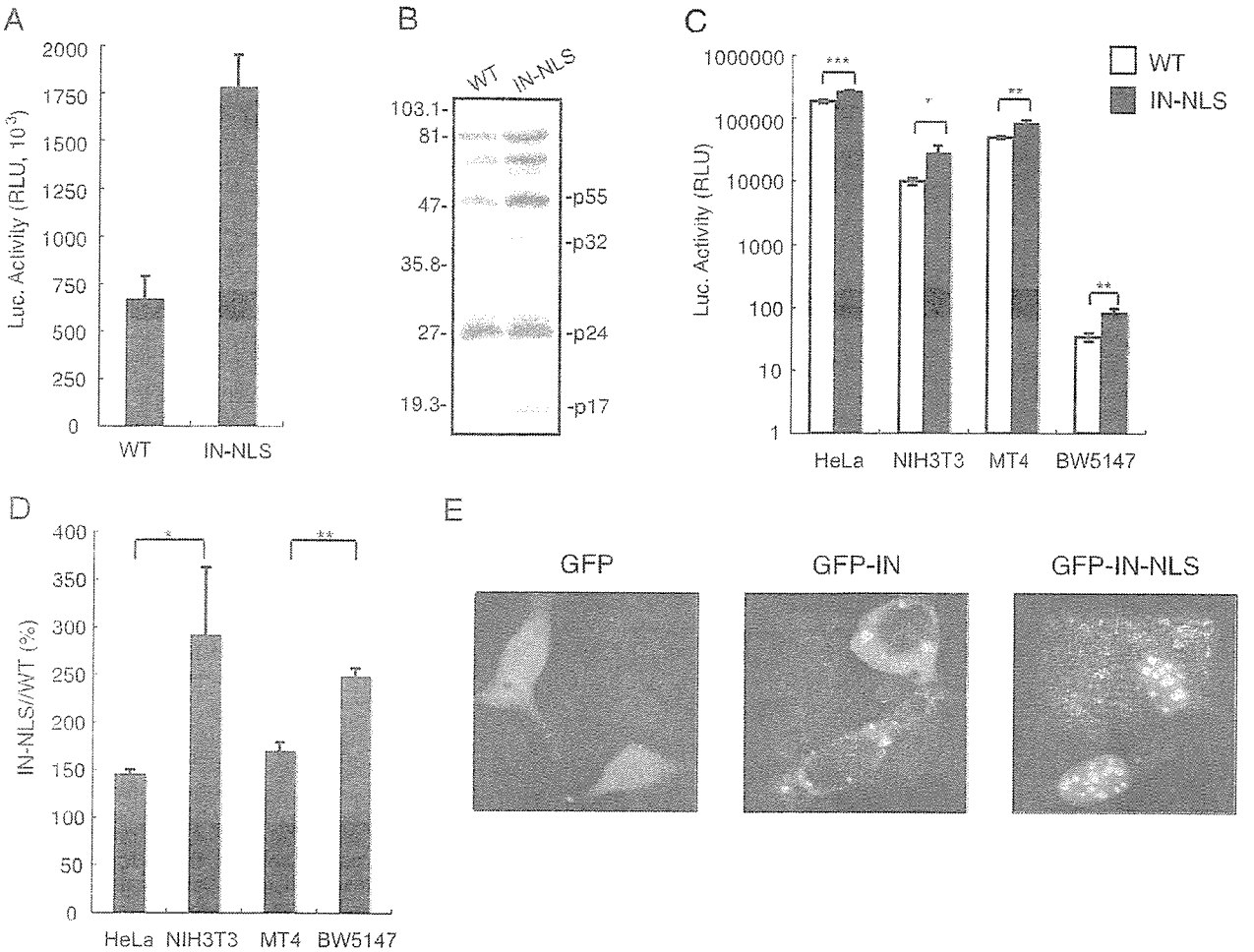

FIG. 8. Enhancement of viral infectivity to mouse cells by the addition of SV40 NLS to the C terminus of IN. (A) Luciferase activity in an HIV-1 pNL43lucΔenv vector (WT) or pNL43lucΔenv vector carrying an SV40 NLS-ligated IN (IN-NLS)-transfected 293T cells were measured at 2 days posttransfection. The data were reproduced in 10 independent experiments. (B) Virus particles were collected at 48 h posttransfection and resuspended in PBS. The viral pellets were hearted at 90°C for 10 min in the presence of sample buffer (62.5 mM Tris-HCl, pH 6.8, 10% glycerol, 2% SDS, 5% 2-mercaptoethanol, 0.005% bromophenol blue). Then viral proteins were electrophoresed on a 12% SDS–polyacrylamide gel. Viral proteins were detected with AIDS patient serum. Positions of the major viral proteins are indicated together with molecular weight markers. (C) Human and mouse cells were infected with equivalent amounts of WT (□) or IN-NLS (■) virus at 37°C for 6 h, and then the virus was removed. The luciferase activity was measured 4 days after infection, and the activity was normalized relative to the total amount of protein. Means ± SEM are shown. (D) Relative Luc activities of IN-NLS virus-infected cells compared to WT virus-infected cells were calculated using the data shown in panel C. Means ± SEM are shown. (E) NIH 3T3 cells transfected with a plasmid expressing GFP, GFP-IN, or GFP-IN-NLS fusion protein were analyzed by confocal microscopy. At 24 h posttransfection, cells were fixed and GFP was detected by a confocal fluorescent microscope. *, $P < 0.05$; **, $P < 0.01$; ***, $P < 0.001$ (by Student's t test).

SV40 NLS to the C terminus of IN significantly enhanced viral infectivity in all cell lines used (Fig. 8C). As the NLS fusion at the C terminus of IN disrupted the *vif* gene, we did not analyze the infectivity to human PBMC, which was nonpermissive to *vif*-deficient virus (24, 69). Interestingly, the effect of the NLS on viral infection was significantly stronger in mouse cells than in human cells (Fig. 8D).

We also analyzed the karyophilic property of GFP-IN-NLS in which EGFP was fused to the N terminus and the SV40 NLS at the C terminus of IN. GFP-IN-NLS accumulated almost exclusively in the nucleus of NIH 3T3 cells, in contrast to GFP-IN (Fig. 8E). These results indicate that the addition of functional NLS to IN compensates the functional defects of IN in mouse cells.

DISCUSSION

HIV-1 replication in rodent cells is blocked at multiple steps, including viral entry, transcription, nuclear export of the mRNA, assembly, and budding (77). In this study, we demonstrated that an additional host range barrier is present in mouse cells at the PIC nuclear transport step. We suggest that this restriction is caused by the dysfunction of the HIV-1 IN-dependent PIC import system.

We found that the ratio of the 2-LTR circular product to the late reverse transcription product (R-gag), which are produced in the nucleus and cytoplasm, respectively, was decreased in mouse splenocytes relative to human PBMCs after infection with both HIV-1/MuLV and HIV-1/VSV-G pseudotyped vi-

ruses (Fig. 6, lower panels). This indicates a reduction in nuclear import of the PIC. The efficiency of nuclear transfer of the viral PIC was recently reported to be reduced in mouse T cells relative to human T cell lines, but not in NIH 3T3 cells (7). These results are consistent with ours, although we cannot explain their lack of reduction in the NIH 3T3 cells. Our system using the IN mutant virus is probably more sensitive in detecting the defect.

We showed that the infection efficiency, as determined by luciferase activity, was 10 to 100, 100 to 1,000, and >1.000 times lower than in human cells in mouse adherent cells, T cell lines, and primary cells, respectively (Fig. 4). As the PIC nuclear import reduction in mouse cells was at most 60 to 90% compared to human cells (Fig. 6), it is clear that other barriers are also involved in the HIV-1 replication restriction in mouse cells. In this regard, we showed that the 2-LTR/R-gag ratio following infection with WT HIV-1 was similar between HeLa and NIH 3T3 cells and between MT4 and BW5147 cells, in contrast to our observations with the IN-deficient mutant virus (Fig. 6, lower panels). These results are explainable if the R-gag products integrate rapidly into the host chromosome in human cells compared to mouse cells, assuming that a constant proportion of free R-gag products is converted into the 2-LTR form. Thus, integration of the R-gag products into the host chromosome may also be inhibited in mouse cells. In accordance with this idea, we demonstrated that the integration frequency of HIV-1 was greatly reduced upon infection with WT HIV-1 in mouse cells transgenic for the huCD4/CXCR4 genes.

There are two formal explanations for the inability of the mouse cells to support HIV-1 PIC nuclear import. One is the absence of a required human-specific factor, and the other is the presence of an inhibitory factor(s) in mouse cells. However, because mouse-human cell fusions allow viral replication, mouse cells most likely do not have such an inhibitory factor and are rather devoid of a critical factor for the import of the HIV-1 PIC (52).

Although the mechanisms of PIC nuclear import have not been elucidated completely, NLSs are present in three viral proteins (MA, Vpr, and IN) as well as in a central DNA flap produced during reverse transcription that also contributes to the successful nuclear targeting of the PIC (59, 64, 71). Although their respective contributions remain controversial and unclear, it has been clearly shown that both Vpr and IN are karyophilic and rapidly accumulate in the nuclei of infected cells (6, 16, 19, 20, 25, 32, 48, 63, 66, 68). Meanwhile, localization of MA to the nucleus is not well established (14, 23). In this report, we demonstrated that GFP-fused IN remained in the cytoplasm of NIH 3T3 cells, in contrast to its accumulation in the nuclei of HeLa cells. On the other hand, when GFP-fused Vprs were examined, they localized to the nuclei of both NIH 3T3 and HeLa cells. The nuclear distribution of GFP-IN, but not GFP-fused Vpr, was also inhibited in the Colon-26 mouse cell line. These observations indicate that Vpr can be imported into the nucleus using separate pathways. IN, on the other hand, cannot be imported efficiently into the nuclei of mouse cells, and this is probably due to the inability of IN to interact with mouse nuclear import system.

In support for this notion, we showed that nuclear import of IN was much more enhanced in mouse cells than in human cells when authentic SV40 NLS was added to IN (Fig. 8). Furthermore, the addition of this NLS to IN significantly enhanced the infectivity of HIV-1 pseudovirus to mouse cells. These results indicate that endogenous nuclear localization signals of IN are not fully functional in mouse cells.

In this context, it is known that the NLSs within HIV-1 IN are composed of basic amino acid-rich sequences that interact with importin β through the adapter importin (25). We previously showed, however, that mutational disruption of the suggested NLSs could not abolish the nuclear localization of a GFP-IN fusion protein (76). Recent studies have shown that nonclassical NLSs are necessary and sufficient to locate the viral PIC into the nuclei (12). Depienne et al. suggested that the in vitro nuclear import of IN does not require known cytosolic transport factors, including karyopherin β family proteins (18). Two proteins have recently been reported to mediate PIC import. The first is lens epithelium-derived growth factor (LEDGF/p75), a protein implicated in the regulation of gene expression and cellular stress responses. LEDGF interacts with HIV-1 IN in vitro and in living cells (50) and colocalizes with HIV-IN in the nuclei of human cells (15). The second is importin 7, a mildly hydrophobic protein belonging to the importin β superfamily. This protein is suggested to interact with basic proteins, such as IN, that bind viral nucleic acids (21). It is currently unclear which protein(s) is important in these processes and defective in mouse cells. Clearly, further work is necessary to identify the host cell factors that are associated with IN in human cells and defective in mouse cells.

Thus far, several host restriction factors are known to be involved in the suppression of HIV-1 replication in the early phase of its life cycle in mouse cells. Friend virus susceptibility factor-1 (Fv-1) is involved in the restriction of specific mouse cell genotypes to MuLV (10, 28). The Fv-1 targets the MuLV capsid and stops the nuclear import of the PIC (8, 39). However, recent reports have noted that there is no correlation between HIV-1 susceptibility and cellular Fv-1 genotype (7, 31). Tripartite motif 5 α (TRIM5α), encoded by the gene *Lv-1*, is another restriction factor (72). TRIM5α inhibits viral replication in rhesus macaque cells at a step after entry but before the reverse transcription of HIV-1 by targeting the viral capsid protein (60). Thus, both Fv-1 and TRIM5α function in processes other than the transport of PIC into the nucleus.

In conclusion, we have demonstrated that PIC nuclear import is blocked in mouse cells and that dysfunctional IN is at least partially responsible for the barrier. Further characterization and identification of factors that are involved in PIC nuclear import should provide new insight into the molecular mechanisms of the PIC import step and clues to the development of new therapeutics. Furthermore, identification of the factors responsible for this step will assist in our generation of transgenic small animal models that are permissive to HIV-1 infection.

ACKNOWLEDGMENTS

We thank Takao Masuda (Tokyo Dental and Medical University) for providing pNL43lucΔenv and an amphotropic Moloney MuLV envelope expression vector (pJD-1) as well as for critical discussions. We also thank Yoshio Koyanagi (Kyoto University) for providing the 2-LTR plasmid and the AIDS patient serum and for important technical advice. We also thank Yoshio Inagaki (Tokyo Medical and Dental University) for providing the AIDS patient serum. We are grateful